Underground Injection Control
Carbon Sequestration
Class VI Permit Application

Area Of Review and Corrective Action Plan
40 CFR 146.84(b)

Section 3.0

TALLGRASS HIGH PLAINS CARBON STORAGE, LLC
WESTERN NEBRASKA SEQUESTRATION HUB

January 2025

Prepared by:

Jessica Gregg (Director, Geoscience Compliance)
Tallgrass High Plains Carbon Storage, LLC
370 Van Gordon St
Lakewood, CO 80228

3.0 AREA OF REVIEW AND CORRECTIVE ACTION PLAN 40 CFR 146.84(b)

WESTERN NEBRASKA SEQUESTRATION HUB

FACILITY INFORMATION

Facility name: Western Nebraska Sequestration Hub
Conestoga I-1

Facility contacts:

Craig Spreadbury | Vice President, Carbon Capture & Sequestration
Tallgrass High Plains Carbon Storage, LLC
370 Van Gordon St
Lakewood, CO 80228
craig.spreadbury@tallgrass.com

Jessica Gregg | Director, Geoscience Compliance
Tallgrass High Plains Carbon Storage, LLC
370 Van Gordon St
Lakewood, CO 80228
jessica.gregg@tallgrass.com

Well location: Kimball County, Nebraska
[redacted]

TABLE OF CONTENTS

LIST OF FIGURES

List of Tables

List of Equations

ACRONYMS AND ABBREVIATIONS

2D	two-dimensional
°F	degrees Fahrenheit
A	
AoR	area of review
API	American Petroleum Institute
B	
bgs	below ground surface
BOP	blowout preventer
BTC	buttress thread coupling
C	
CBW	clay-bound water
CMG	Computer Modeling Group
cmt	cement
CO_2	carbon dioxide
cP	centipoise
CRA	Crushed Rock Analysis
Csg	casing
E	
EOI	end of injection
EOS	equation-of-state
EPA	U.S. Environmental Protection Agency
F	
ft	feet/foot
°F/ft	degrees Fahrenheit per foot
G	
gal	gallon
GR	gamma ray
GSDT	Geologic Sequestration Data Tool
H	
HPA	High Plains Aquifer
I	
ID	inner diameter
in.	inches
K	
KB	Kelly bushing
k_v/k_h	vertical to horizontal permeability ratio
L	
lb	pounds
lbf	pounds force
lbm	pounds mass
lbm/ft^3	pounds mass per cubic foot

M	
mD	millidarceys
mg/L	milligrams per liter
MMSFC	million standard cubic feet
MMscf/D	million standard cubic feet per day
Mt	Million metric ton
Mta	Million metric tons per annum
MULTPV	pore volume multiplier
N	
NAD	North American Datum
O	
OD	outer diameter
P	
Project	Western Nebraska Sequestration Hub
psi	pounds per square inch
psi/ft	pounds per square inch per foot
R	
RCAL	Routine Core Analysis
Reference Wells	[redacted]
S	
SH	shale
sk / sx	sack(s)
SS	sandstone or subsea
T	
TH.	thickness
TVD	true vertical depth
TVDSS	true vertical depth sub-sea
TDS	total dissolved solids
TVT	true vertical thickness
U	
UIC	Underground Injection Control
USDW	underground source of drinking water
V	
kv/kh	vertical-to-horizontal permeability ratio
v/v	volume per volume
W	
WOB	weight on bit
WOC	weight on cement
WT	weight
X	
XRD	x-ray diffraction

3.0 AREA OF REVIEW AND CORRECTIVE ACTION PLAN [40 CFR 146.84(B)]

3.1 Computational Modeling Approach

3.1.1 Modeling Approach

Tallgrass High Plains Carbon Storage, LLC (High Plains) proposes drilling and completing a carbon sequestration injection well (Conestoga I-1) and monitoring well (Conestoga M-1) for the safe sequestration of carbon dioxide (CO_2) in southeastern Kimball County, Nebraska, as part of their proposed Western Nebraska Sequestration Hub (the "Project"). The Juniper M-1 well (API No. 49-021-29548) is utilized as the Project's characterization well (**Figure 3.1**).

Estimating key subsurface parameters affected by the injection of supercritical carbon dioxide into the Lyons Formation is the principal focus of the static geologic modeling effort and the dynamic reservoir simulation model. These subsurface parameters include changes in reservoir pressure and injectate (gas) saturation[1] following the start of injection—assumed as January 2027 in the model. These parameters provide critical insights across the Project area and help to define the extent of the resulting injectate plume, pressure propagation (and the resulting pressure front), and operating conditions. These outputs are then utilized to determine the Project's Area of Review (AoR). Industry-standard software tools, including SLB's Petrel™ and the Computer Modelling Group's (CMG) GEM™, were used to provide accuracy and reliability in managing the complex nature of the simulation.

A representation of the reservoir was constructed from available well logs and interpreted formation tops (refer to **Appendix 3.1** for a list of wells and markers used to construct the regional geologic model). Subsurface data was modeled using SLB's Petrel™ software to form a static geocellular model of discrete zones, including the Lyons Formation (injection zone), Goose Egg Formation (upper confining zone), and Satanka Formation (lower confining zone). The geocellular model used for dynamic simulations (the "dynamic grid") is comprised of approximately 31.6 million 1,000×1,000 ft cells and encompasses an area of 12,300 square miles.

The geologic model is an input for GEM™, a commercial compositional finite difference reservoir simulator maintained and distributed by CMG. This simulator is one of the most technically sound reservoir simulation software packages and is well suited to the compositional nature of this simulation. CMG-GEM™ utilizes equation-of-state (EOS) algorithms and advanced computational methods to evaluate key fluid flow characteristics in the reservoir to produce accurate and dependable simulation models for carbon sequestration. Numerical simulations were run to forecast the subsurface behavior of supercritical CO_2, pressure buildup from CO_2 injection,

[1] The injectate stream, primarily composed of CO_2 gas at standard pressure and temperature, is modeled in the subsurface under conditions above the critical point. At the modeled reservoir conditions, the CO_2 exists in a supercritical phase. The simulator tracks the inventory of CO_2 mass and other components of the injectate stream within the model domain, categorizing them as "gas" properties. The behavior of CO_2 in the subsurface is calculated using properties consistent with the supercritical phase. Therefore, when gas saturation is mentioned in this context, it refers to the saturation of the entire injection stream, which remains in the supercritical phase within the reservoir.

and output parameters, such as pressure and injectate saturation, used to evaluate and establish the Project's AoR.

Core samples and well log data were collected across the injection and confining zones in the Juniper M-1 well to directly measure relative permeability, porosity, capillary pressure, and the geomechanical properties of the Lyons, Goose Egg, and Satanka.

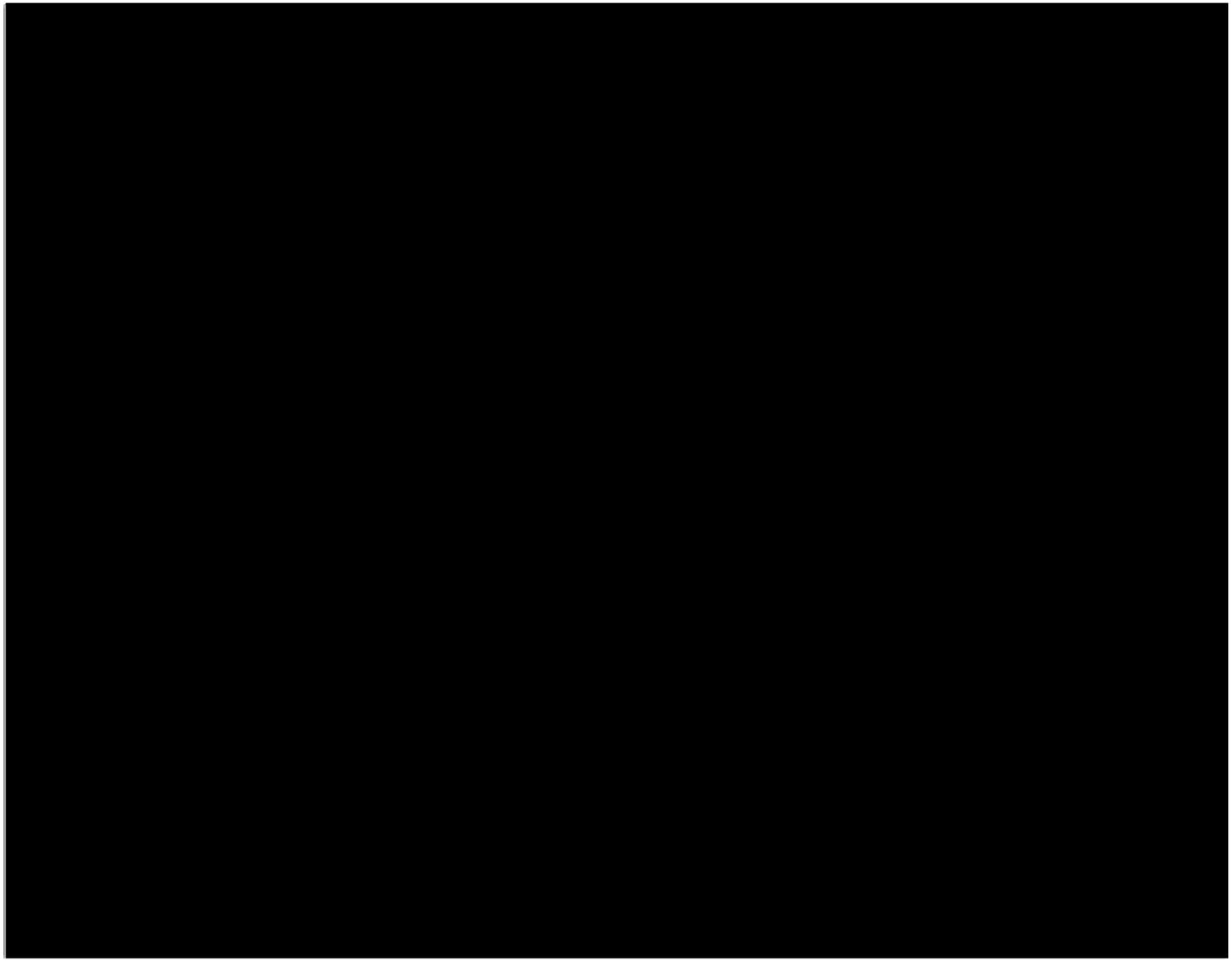

Figure 3.1—Map displaying the Project's characterization well, the Juniper M-1 (API No. 49-021-29548), and the Reference Wells (see *Section 2.4*), in relation to the proposed Conestoga I-1 injection well and the AoR.

3.1.2 Site Geology and Hydrology

The model domain is located in the Denver-Julesburg (DJ) Basin, an asymmetric synclinal basin bound by Laramide tectonically-driven uplifts of the Rockies Front Range and Hartville Uplift to the west, the Chadron and Cambridge Arches to the north and east, and the Las Animas Arch and Ute Pass Fault Zone to the south (**Figure 3.2**). The model encompasses the northern central part of the basin from the basin axis in the west to the inferred basin boundary in the east. Twenty-eight stratigraphic horizons, ranging in age from Pennsylvanian to Tertiary, were mapped across the basin utilizing log data from 433 wells, totaling over 7,200 well formation tops that were used to characterize structural and stratigraphic trends. However, only four of these horizons were incorporated into the static geomodel, as they represent the primary injection and confining zones. 2D seismic data was licensed across the model domain and AoR and was incorporated into the structural modeling to confirm basin structural configuration and evaluate if faulting is present. Definitive geophysical and geological horizons exhibit significant character changes northwest of the model domain, corroborating the northwest basin boundary described in literature (Oldham, 1997). The licensed 2D seismic across the Project area confirms reservoir and confining zone continuity and the absence of faulting from the storage complex.

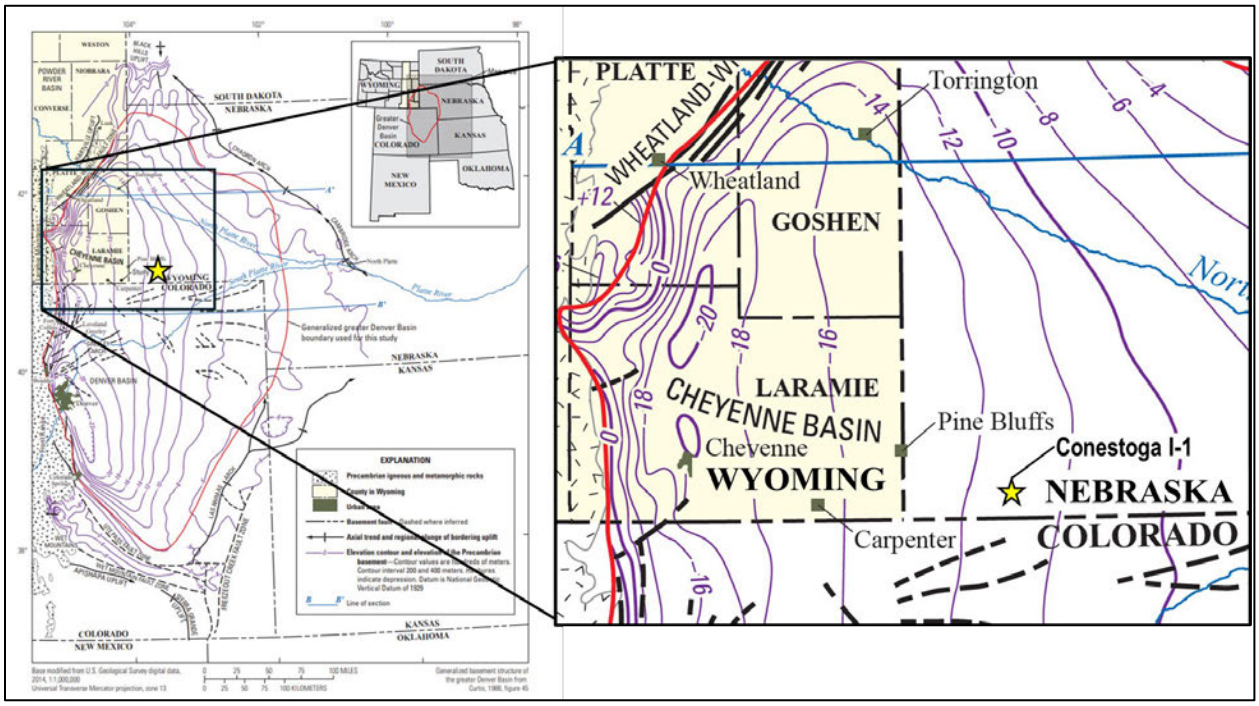

Figure 3.2—Generalized basement structure of the greater DJ Basin in Wyoming, Nebraska, Colorado, and Kansas (after Bartos et al., 2021). The yellow star is the approximate location of Conestoga I-1. Note there is no interpreted faulting within the AoR.

Lyons Formation – Injection Zone

The Lyons Formation is an ideal reservoir for sequestering CO_2. The Permian-age Lyons Formation is a well-sorted quartzose eolian sandstone deposited as part of a widespread dune field covering a large portion of the eastern Rockies region adjacent to the Ancestral Rockies. A

predominant wind direction blew sediment from east-northeast to west-southwest (**Figure 3.3** and **Figure 3.4**).

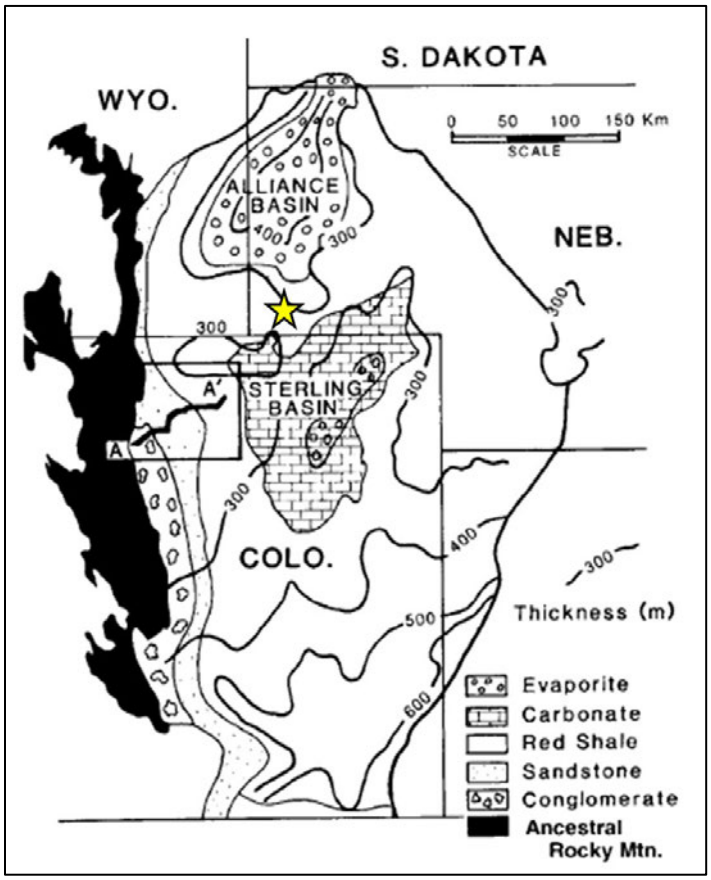

Figure 3.3—Regional isopach map of the Lyons Formation, identifying Alliance and Sterling Basins (after Lee and Bethke, 1994). The yellow star is the approximate AoR location.

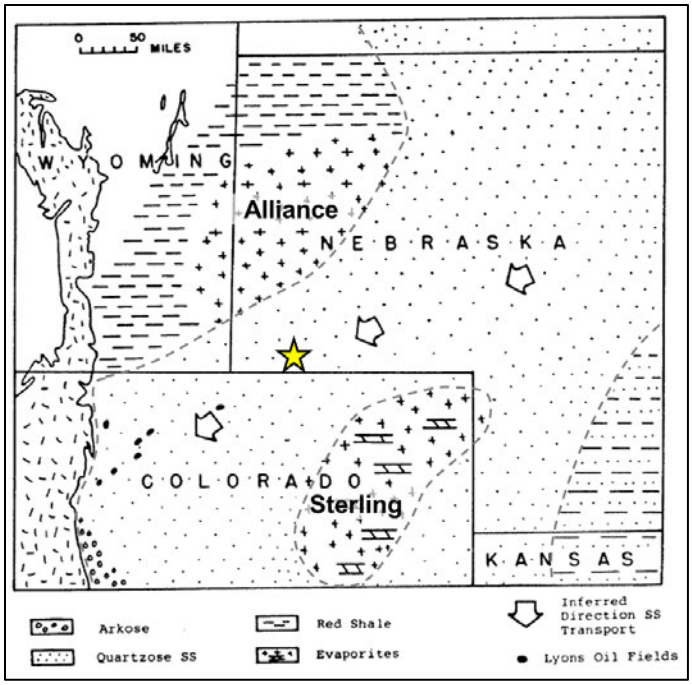

Figure 3.4—Regional lithofacies and paleo wind direction map of the Lyons Formation. The yellow star is the approximate location of the AoR (after Sonnenberg, 1981).

At the time of deposition, the Lyons eolian dune field was bounded to the north by the Alliance Basin and partially to the south by the Sterling Basin. These evaporite sabkha basins deposited thick sequences of anhydrite, siltstone, dolomite, and salt adjacent to the Lyons dune accumulation, leading to a lateral facies change into the time-equivalent Stone Corral Formation (also known as the Salt Plain Formation) (Oldham, 1996; Sonnenberg, 1981) (see **Figure 3.5**). Extensive mapping of these facies transition boundaries indicates that the Lyons Sandstone grades into the sabkha basins evaporites. To simplify modeling this regional transition, which occurs well outside the AoR, the relationship has been represented as a surface truncation of the Lyons Formation onto the underlying Satanka Formation.

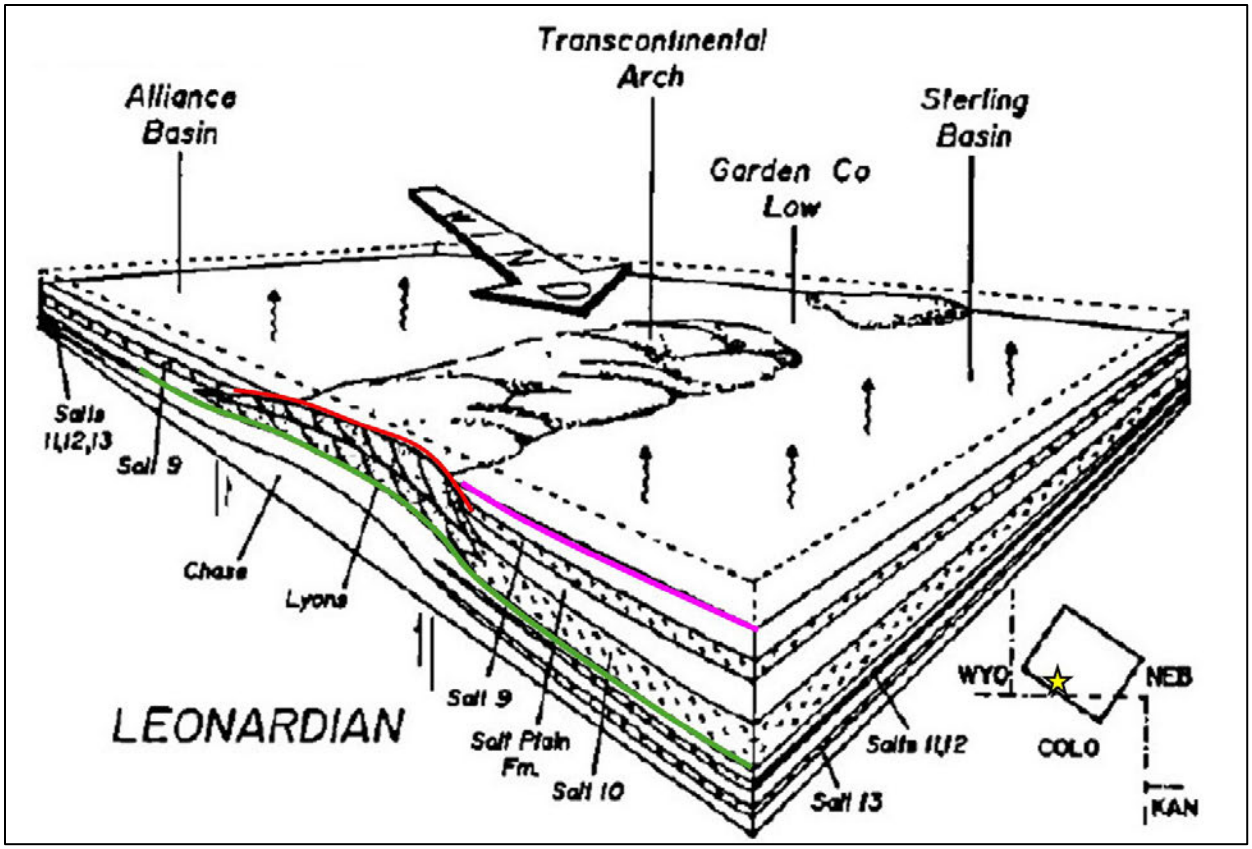

Figure 3.5—Block diagram depicting the facies changes within the Lyons Formation (Oldham, 1997). The green surface represents the Satanka Formation, as shown in the generalized stratigraphic column in *Section 2*. The red surface indicates the Lyons eolian sandstone surface, and the pink surface represents the Stone Corral Formation, a time-equivalent lateral facies changes from the Lyons eolian sandstone to the Sabkha basin facies of the Alliance and Sterling basins.

The Alliance Basin acts as a partial lateral barrier to fluid flow, extending across part of the northern DJ Basin. Similarly, the Sterling Basin is a partial lateral flow barrier to the south. However, the evaporite deposits do not extend across the entire DJ Basin, and the Lyons eolian sands are known to be connected further southward around the smaller Sterling Basin (**Figure 3.4**).

The Lyons Formation has been extensively studied both at outcrops along the Rockies Front Range in Lyons, Colorado, and through numerous cores obtained from oil-producing fields in Weld County, Colorado (Sonnenberg, 1981; Kendigelen et al., 2023).

Petrographic and geochemical analysis of Lyons outcrop and core samples indicate that the zone is a relatively homogenous quartzose sandstone across the model domain. High Plains does not anticipate adverse chemical reactions in the Lyons Formation from CO_2 injection (see *Section 2.8—Geochemistry*). The framework grain mineralogy is largely non-reactive or has very slow kinetics under injection conditions (Black et al., 2015; Palandri and Kharaka, 2004).

The Lyons Formation outcrops along the Rockies Front Range and steeply dips into the DJ Basin synclinal axis, reaching depths greater than 10,900 ft true vertical depth (TVD). The structure of the DJ Basin and the Lyons Formation gently dips westward at an angle of less than two degrees (**Figure 3.6**). At the Conestoga I-1 location, the Lyons is expected to be penetrated at a depth of

approximately [redacted] with a thickness of [redacted] ft (**Figure 3.7, Figure 3.8**). One well penetrating the Lyons Formation exists within the AoR, the [redacted]. The openhole log in this well indicates the Lyons has a gross true vertical thickness (TVT) of [redacted] ft (**Figure 3.8**). Lyons thickness ranges from 0 to 620 ft thick across the DJ Basin (**Figure 3.3**). Across the model domain, the gross thickness (TVT) of the Lyons ranges from [redacted] with a range of [redacted] ft within the AoR (**Figure 3.7**). Locally observed mapped thickness changes are attributed to preserved dune geometry, which can create large local disparities in thickness from dune crests to troughs. Based on a review of all applicable data, no structural or stratigraphic barriers are present within the AoR. In the AoR, the Lyons dips gently (less than one degree) towards the west, and no faults or folds have been identified with the available data.

Figure 3.6—Top Lyons Formation structure contour map with all well control points (red) used to generate the surface. Red dots and associated numbers are the TVDSS depth (ft) values for each respective Lyons Formation top. The yellow star indicates the proposed Conestoga I-1 location within the AoR boundary (blue).

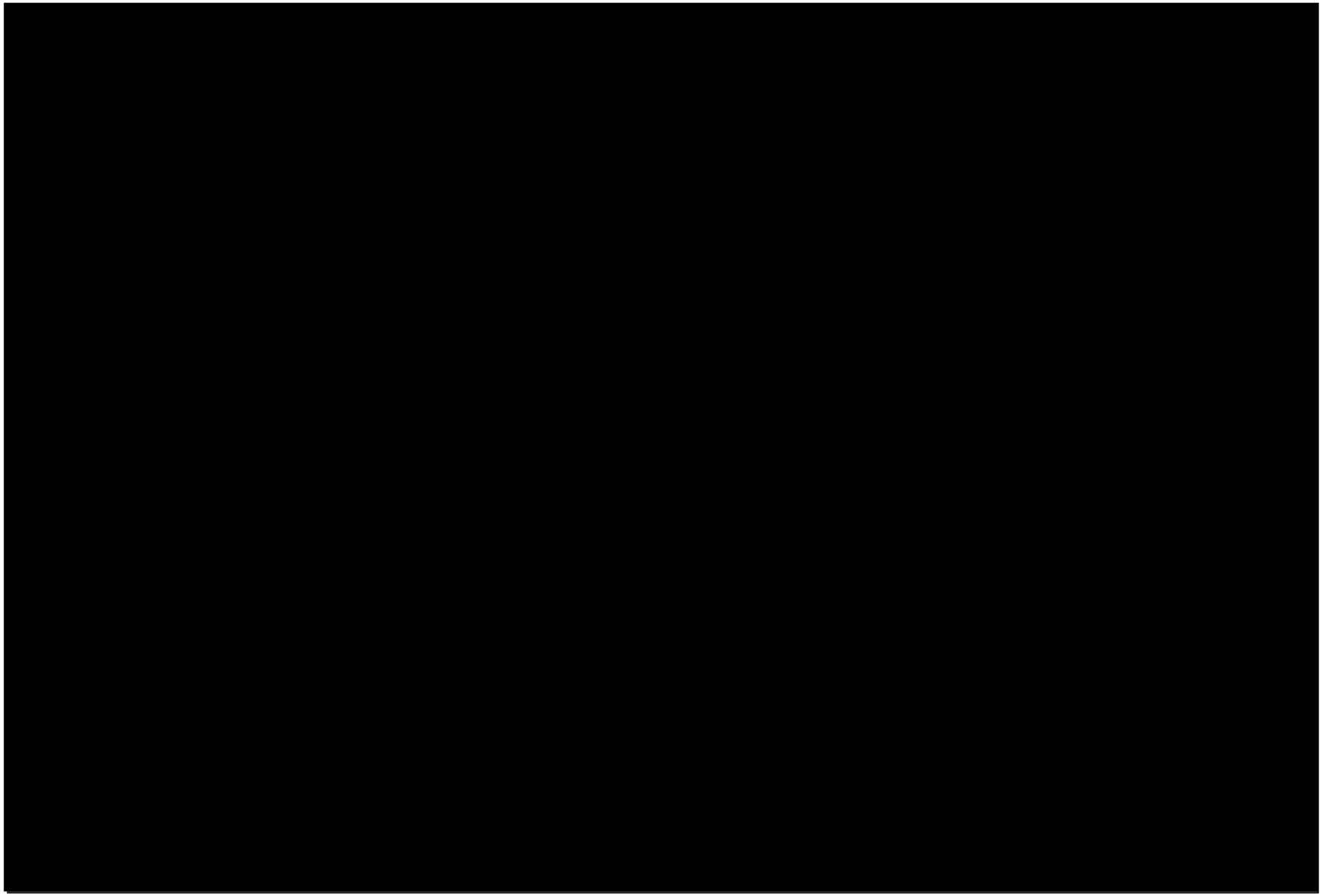

Figure 3.7—Lyons Formation gross thickness (TVT) isochore map with all well control points used to generate the surface. Red squares and associated numbers are the thickness values for each Lyons-to-Satanka isochore point. The yellow star indicates the proposed Conestoga I-1 location within the AoR boundary (blue).

Figure 3.8—Type log from the [redacted] located [redacted] miles from the proposed injection site. The log columns indicate the injection zone and confining intervals, their reservoir quality with respect to porosity (PHIE), and their associated general lithology. The far-left column displays gamma ray increasing from left to right with a range of 0 to 150 API. Effective porosity is displayed in the middle-right column, increasing from right to left from 0 to 30%. The thin column on the far right is a generalized lithology log showing each stratigraphic zones respective lithology (brown – shale, yellow – sandstone, red – siltstone, pink – evaporite, blue – dolomite/limestone). The yellow star on the location map indicates the proposed injection site (Conestoga I-1) and the red star indicates the [redacted] well location.

Goose Egg Formation – Upper Confining Zone

The upper confining zone for the project is the Goose Egg Formation. The Goose Egg was deposited in a shallow, widespread evaporite basin characterized by red-bed muddy siltstone and limestone sheets, interbedded with massive gypsum layers that later converted to anhydrite in the subsurface. The Goose Egg Formation spans the DJ Basin, filling in the preserved dune topography of the Lyons Formation. Sediment was sourced from the Ancestral Rockies to the west, while the restricted sabkha basin environment precipitated thick in-situ evaporite deposits (**Figure 3.9**). Log and core data indicate consistent physical properties of the Goose Egg Formation across the DJ Basin and the Area of Review (AoR).

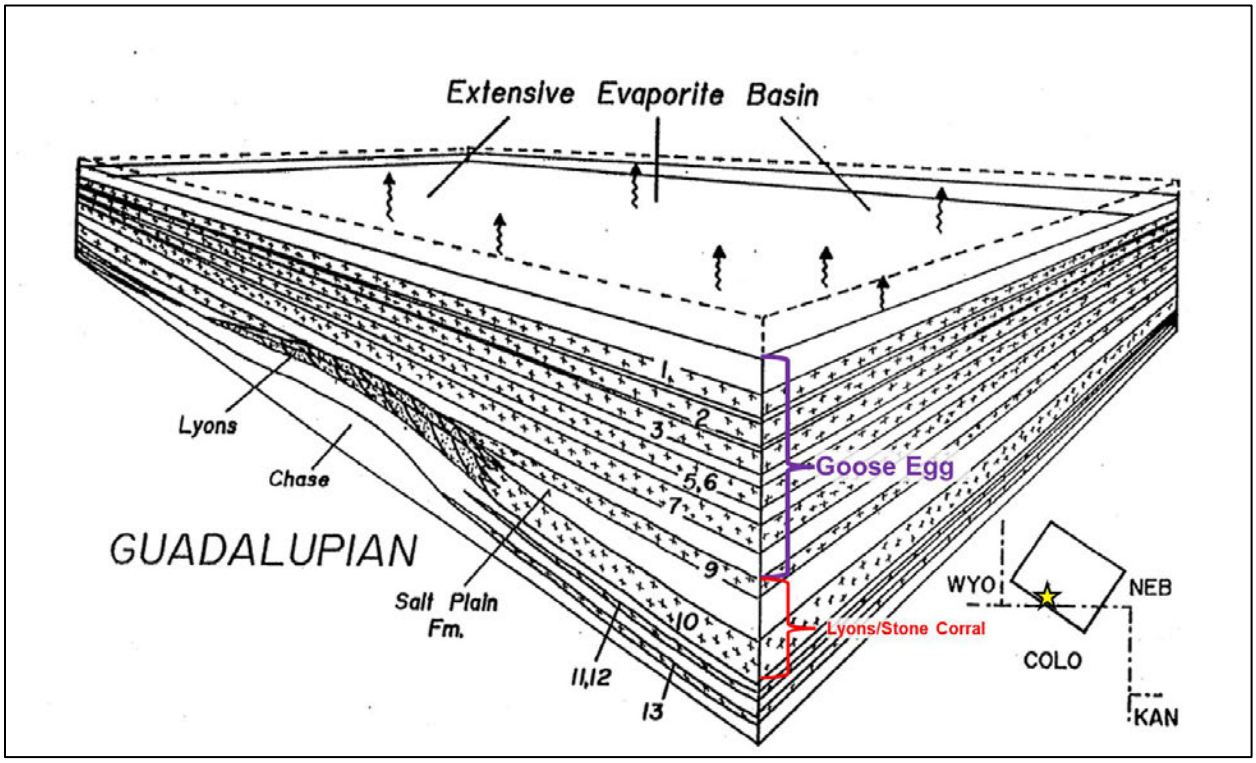

Figure 3.9—Block diagram of Goose Egg (Late Permian Guadalupian) deposition over the Lyons Formation at the Project site (yellow star; after Oldham, 1997).

The Goose Egg outcrops to the east of the Rockies Front Range and steeply dips into the DJ Basin synclinal axis, reaching depths greater than 10,600 ft TVD. The structure of the DJ Basin, and consequently the Goose Egg Formation, dips gently to the west at less than two degrees (**Figure 3.10**).

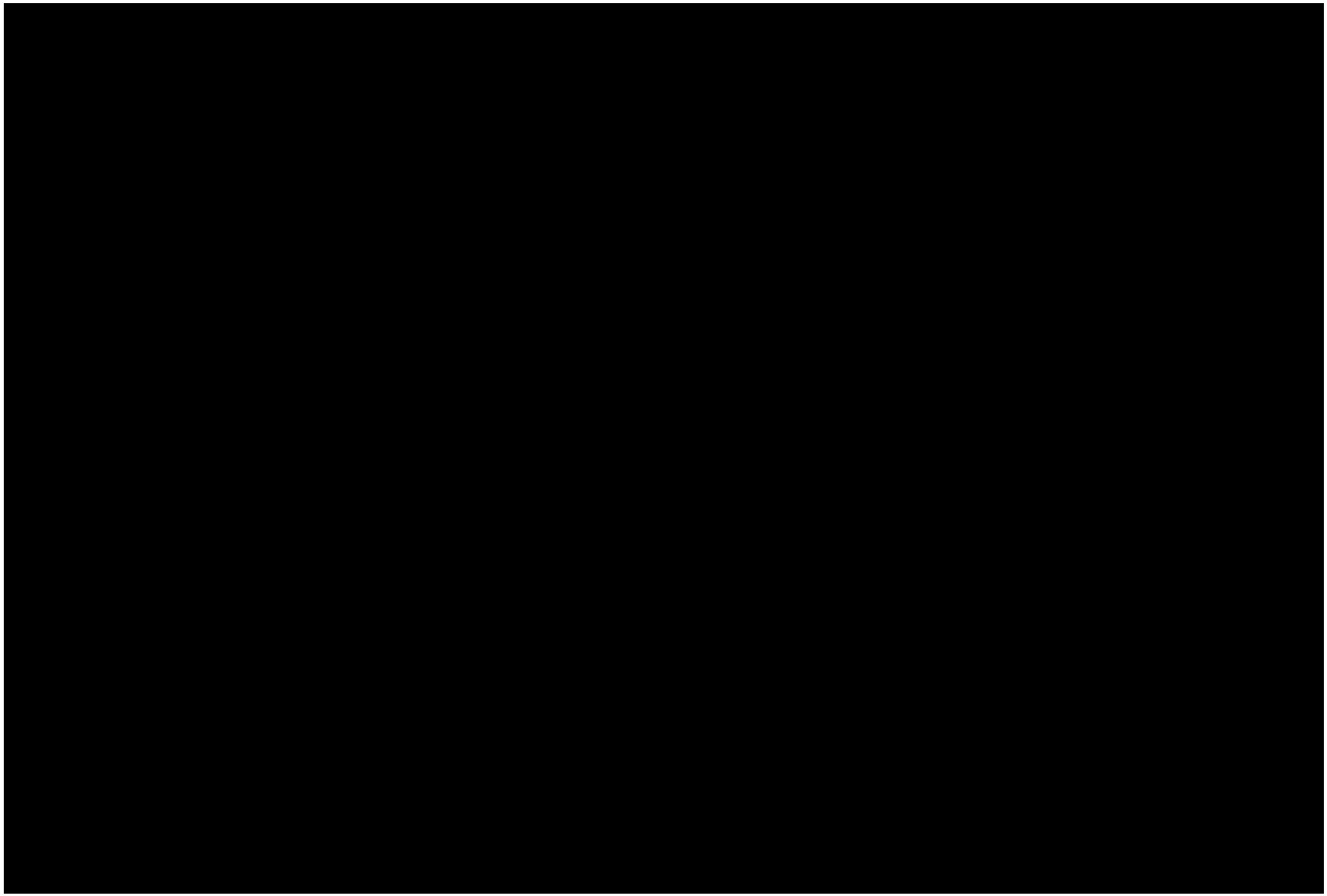

Figure 3.10—Top Goose Egg Formation structure contour map with all well control points used to generate the surface. Purple dots and associated numbers are the TVDSS depth values for each Goose Egg top. The yellow star indicates the proposed Conestoga I-1 location within the AoR boundary.

At the Conestoga I-1 location, the Goose Egg is expected to be encountered at a depth of approximately [redacted] with a thickness (TVT) of [redacted] ft. One well penetrating the Goose Egg exists within the AoR, the [redacted] which is [redacted] miles from the proposed Conestoga I-1 location. At [redacted] the Goose Egg gross thickness (TVT) is [redacted] ft (**Figure 3.11**). Across the model domain, the Goose Egg Formation's gross thickness (TVT) ranges from [redacted] ft, and from [redacted] ft within the AoR, depending on the relict topography of the underlying Lyons paleo-dunes. The Goose Egg Formation appears to thicken in areas where the underlying Lyons Formation thins (**Figure 3.11**).

Figure 3.11—Goose Egg gross thickness (TVT) isochore map with all well control points used to generate the surface. Purple squares and associated numbers are the thickness values for each Goose Egg-to-Lyons isochore point. The yellow star indicates the proposed Conestoga I-1 location within the AoR boundary (blue).

Satanka Formation - Lower Confining Zone

The lower confining zone is the Satanka Formation, which was deposited in a more arid environment than the Goose Egg, which accounts for a larger percentage of fine-grained siltstones and only minor anhydrite bedding. Similarly, the Satanka was deposited in an arid, flat, and broad salt playa delta with minor geomorphological highs and lows within the model domain. Log and core data indicate that the Satanka Formation is continuous across the model domain.

Hydrology and USDWs Summary

The lowermost USDW is expected to be the High Plains Aquifer (HPA) at the Project site. Structure maps for both the base of the HPA and the top water level have been georeferenced and incorporated into the regional conceptual model (Sibray et al., 2020; Miller and Appel, 1997). In addition to the Goose Egg Formation upper confining layer, thousands of feet of competent low permeability shale formations separate the Lyons Formation injection zone (approximately [redacted] ft TVD) and the base of the lowermost USDW (approximately [redacted] ft TVD). This thick sequence of Cretaceous shales and mudstones further reduces the risk of vertical migration of CO_2 or formation fluids from the injection zone to a USDW through a geologic pathway.

Sections 2.1, 2.2, and *2.7* of this application discuss further details of site geology and hydrogeology at length.

3.1.3 Model Domain

3.1.3.1 Static Model Summary

The static geologic model was generated in SLB's Petrel™ software and covers an area of 12,300 sq miles across the central-northern DJ Basin (**Figure 3.12**). The model domain was oriented and sized in such a way as to cover the full range of the Lyons regional eolian dune trend between the Alliance and Sterling basins in the northern DJ Basin. The static geomodel was cropped to a smaller representative area of 5,900 sq miles for dynamic simulation. The static geomodel was built using a grid sizing of 1,000×1,000 ft that was rotated N65 degrees E to best match the orientation of the Lyons eolian trend. High Plains determined that a grid size of 1,000×1,000 ft adequately represents the regional geology given the size of the model (12,300 sq miles) and well control spacing.

Figure 3.12—Model domain basemap indicating the approximate DJ Basin outline, static geomodel domain, and dynamic simulation model domain. Red squares represent surface picks. Blue squares represent wells with adequate log suites used for petrophysical analysis (these also have Lyons top picks). The proposed injection site is located by the yellow star.

The static geomodel consists of 802×443 (I×J) cells and 89 layers (K) for a total cell count of 31,620,454 cells (I×J×K).

Initial mapping stages included correlating formation tops using digital well logs for 433 wells across the DJ Basin, 331 of which are inside the regional model domain. Well log formation tops were the primary data used to generate the stratigraphic framework.

Petrophysical analysis was conducted on [redacted] wells within the model boundary to determine each stratigraphic zone's porosity, permeability, and salinity. Proprietary 3D seismic data in an adjacent county east of the Area of Review (AoR) provided high-resolution imaging of a complete dune body, revealing its size and orientation. This information was used as an analog to inform the variogram in the petrophysical model, ensuring a more accurate representation of the dune bodies within the Lyons Formation.

The core description of the Juniper M-1 stratigraphic test well identified two distinct sand facies within the Lyons Formation, designated as "A" and "B." These facies differ in mineralogy and permeability. High Plains utilized gamma-ray response to differentiate between Facies A and B. The RCAL porosity and permeability data indicated distinct porosity-permeability relationships in each facies, further discussed in *Section 3.1.3.1.4—Matrix Permeability*. For the Goose Egg and Satanka formations, crushed rock analysis (CRA) of low-permeability rocks was employed to assign a single transform for the confining zones.

3.1.3.1.1 Structural Framework

The structural framework model for the northern-central portion of the DJ Basin was developed using well-log picks, correlated from both digital and raster logs across the model area.

Formation tops were picked from the ground surface down to the Wolfcamp Formation, which marks the base of the Satanka Formation, with particular attention to the Sundance Formation and deeper layers (**Figure 3.8**). The structural horizon for the Lyons Formation was generated using 433 log markers (**Appendix 3.1**, **Figure 3.13**). These stratigraphic markers served as data constraints for generating stratigraphic surfaces, or horizons, which form the foundation of the static geologic model.

Several iterations of quality control were incorporated to ensure well elevations were correct, log picks and correlations were geologically sound, and the generated surfaces honored selected tops at each well location. In areas with limited data control for deeper formations conformal gridding methodology utilizing isochores was applied to retain structural concordance with overlying well-constrained horizons.

Figure 3.13—Top Lyons structural contours within the regional static geologic model domain. Red squares represent stratigraphic marker tops. Blue squares represent wells with adequate log suites used for petrophysical analysis (these also have Lyons surface picks). The proposed injection site is located by the yellow star.

The top of the Lyons Formation horizon was generated using conformal gridding above the existing Satanka surface, guided by the Lyons-to-Satanka isochore thickness map, and constrained to honor well tops at their respective locations. Within the isochore interpolation process, a zero thickness pinch out was incorporated to represent the line at which the Lyons Sandstone undergoes a facies change to the evaporite-rich Stone Corral Formation of the Alliance and Sterling basins. This isochore map was then used in the conformal gridding algorithm to generate a top Lyons surface that truncates onto the Satanka horizon (gridded as "base surface") to best represent the stratigraphic relationship shown in **Figure 3.5**.

Structural surfaces were generated for all key intervals from the ground surface to below the base of the Lyons Formation. However, petrophysical modeling and the regional model incorporated only the Goose Egg Formation (upper confining zone), Lyons Formation (injection zone), and Satanka Formation (lower confining zone) (**Figure 3.8**). The Wolfcamp surface was gridded and incorporated into the model without petrophysical interpretation to serve as the base layer for the Satanka zone.

3.1.3.1.2 Layering

Proportional model layers (k-layers) were generated for the Goose Egg and Satanka Formations, with each subdivided into three layers to capture vertical variability within the zones. The Lyons zone was layered using the "follow base" method with three-foot thick layers to represent first-order surfaces of interdune strata. These interdune beds can appear as laterally or vertically confining zones of lower-angle bedding with unknown continuity.

The static model includes 89 layers, 83 of which are in the Lyons Formation, and a total cell count of 31,620,454.

3.1.3.1.3 Porosity Model

The available pore volume in the Lyons Formation controls the volume of CO_2 that can be stored in the reservoir and is fundamentally related to permeability. High Plains is updating the petrophysical modeling across the basin by incorporating additional data from the Juniper M-1 core. Petrophysical modeling within the AoR has updated petrophysical models (as described in *Section 2.4*) and the current working petrophysical models within the geomodel. In both petrophysical total porosity models, small mineralogic changes within the Lyons Formation are considered with log responses that predict porosity. A comparison of the total porosity between the original ELAN and the deterministic modeling shows negligible differences (±0.01 v/v).

Modeling updates will continue as additional site-specific data is collected. The current petrophysical model for porosity is based on density, neutron, and sonic porosity logs from 266 wells within the static model domain, which were used to model the regional effective porosity of the injection zone.

Porosity and permeability were evaluated using SLB's Petrophysical software package Techlog™. The Quanti.Elan™ module, a mineralogical inversion application, was employed to provide a quantitative formation evaluation of openhole logs, level by level. The evaluation optimizes simultaneous equations describing one or more interpretation models, with input variables, primarily well logs, used to solve for the desired mineral outputs and volumes. These outputs are

then used to compute additional petrophysical properties such as total and effective porosity. Given the low clay content in most wells across the basin, total and effective porosities are approximately equal in the Lyons Formation.

From the inversion model outputs, total porosity (**Equation 3.1**) is calculated by summing the total volumes of water and gas in the system. Effective porosity (**Equation 3.2**) is total porosity minus the clay-bound water (CBW) and the capillary-bound water.

Equation 3.1—Total porosity.

$$PHIT = 1 - (V_{qtz} + V_{cly})$$

Where:

PHIT = Total Porosity (v/v)
V_{qtz} = Quartz Volume (v/v)
V_{cly} = Clay Volume (v/v)

Equation 3.2—Effective porosity.

$$PHIE = PHIT - CBW$$

Where:

PHIT = Total Porosity (v/v)
PHIE = Effective Porosity (v/v)
CBW = Clay bound water (v/v)

The highest quality Lyons rock is in Kimball County, Nebraska and Laramie County, Wyoming, in the center of the interpreted dune field where thickness and effective porosity are high, as shown by modeled porosity times thickness (PHI×H) (**Figure 3.14**) and average porosity (**Figure 3.15**) maps. Because no core data are available within the AoR, at least one future well will be cored within the AoR to evaluate the upper confining and injection intervals.

The static and dynamic models will be updated with data obtained from the Conestoga I-l.

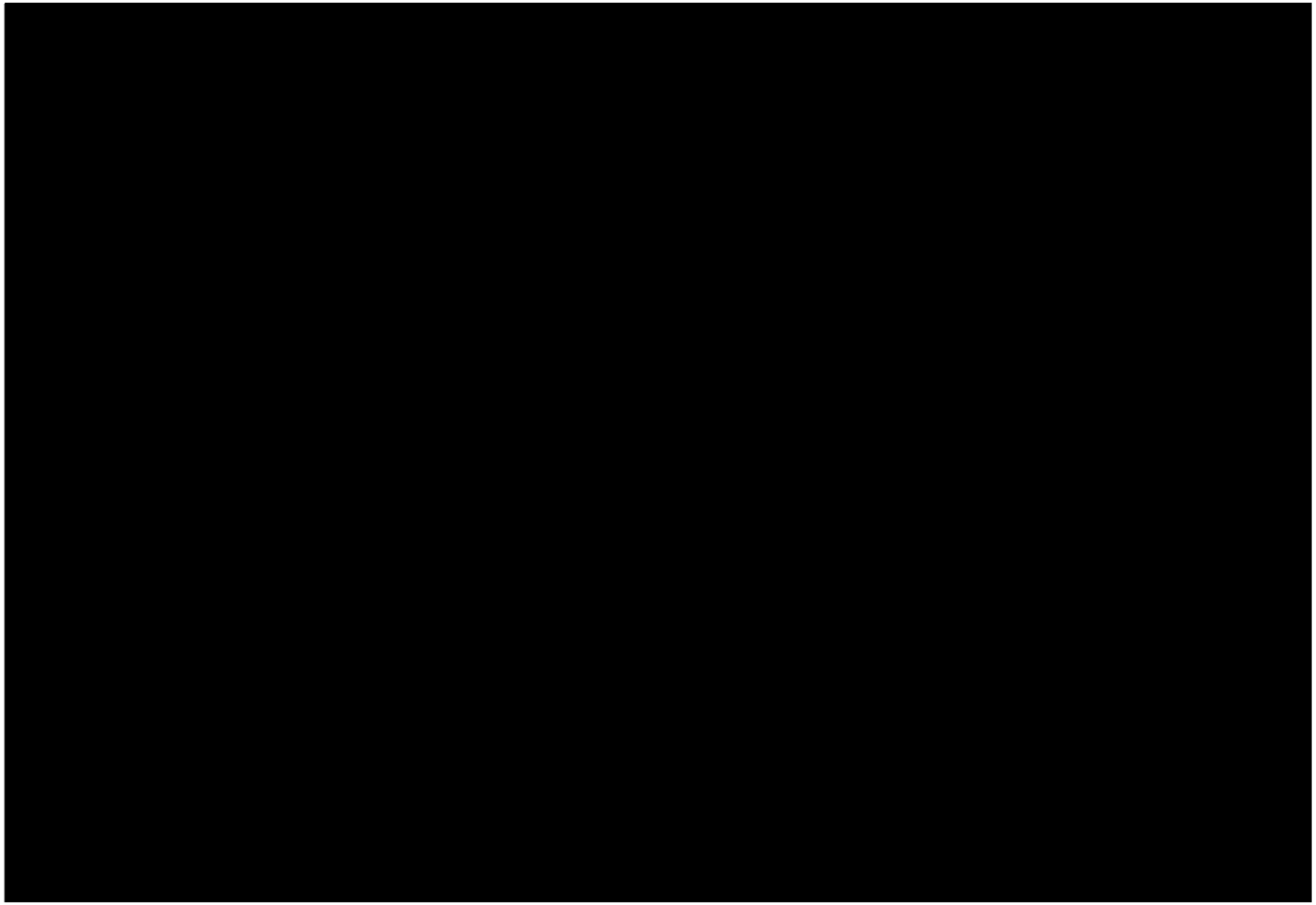

Figure 3.14—Lyons porosity-height (PHI×H) map. This map was generated by the petrophysically modeled PHIE property multiplied by gross thickness within each cell. This map highlights the distribution of Lyons rock quality and pore volume across the northern DJ Basin.

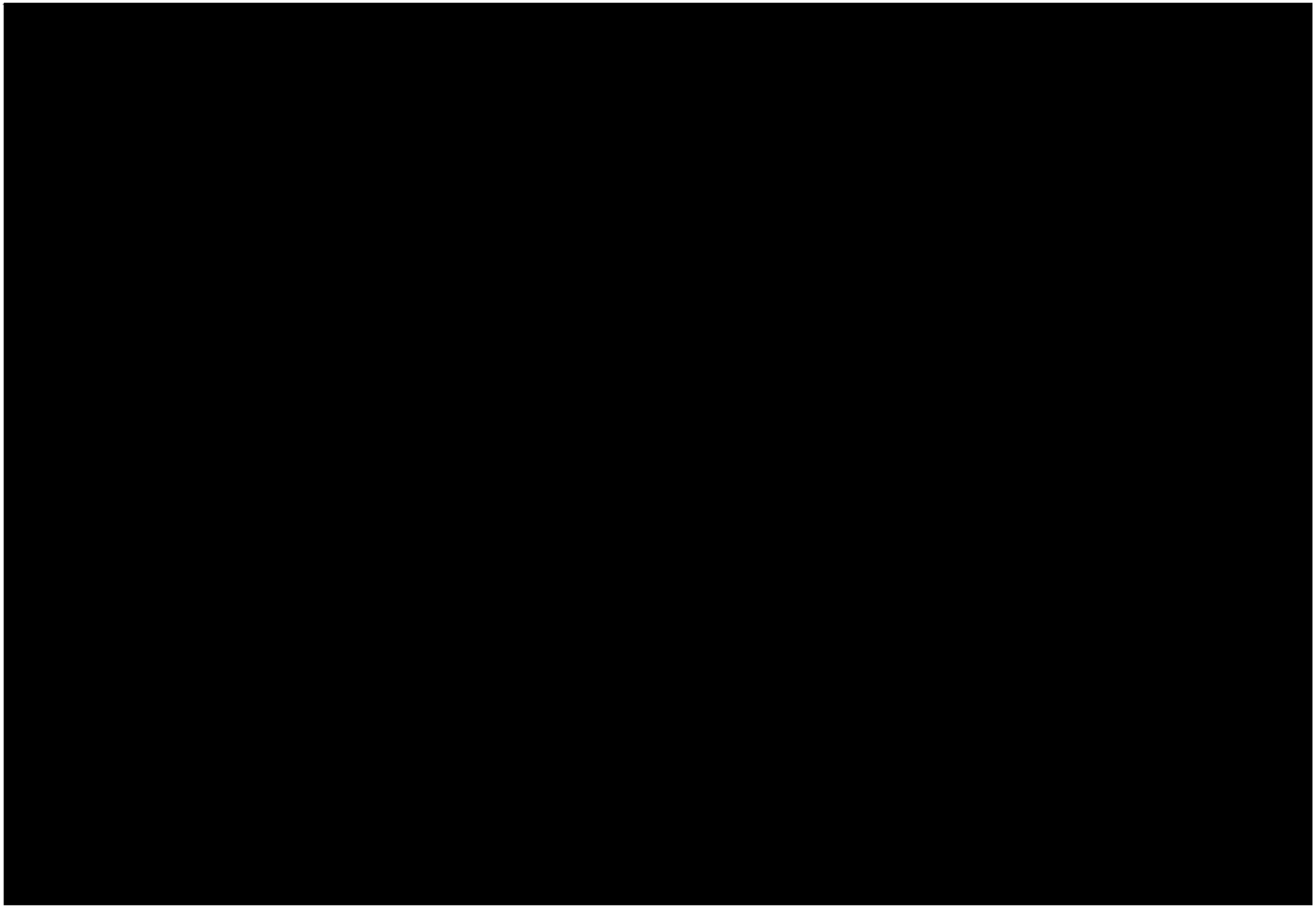

Figure 3.15—Lyons Formation average effective porosity map. This map was generated by vertically averaging the petrophysically modeled PHIE property multiplied by gross thickness within each cell. This map highlights the distribution of Lyons' average porosity across the northern DJ Basin. The data control points are the blue squares, representing wells with petrophysical PHIE interpretation.

Effective porosity values, derived from petrophysical logs in [redacted] wells (**Appendix 3.1**), were upscaled into the model grid by averaging the log values that intersected each model cell. In the clay-poor Lyons Formation, total and effective porosity (i.e., porosity that takes non-contributing clay porosity into account) are equivalent. After upscaling, porosity was distributed across the model using controls specifically designed to reflect the characteristics of the dune bodies, ensuring that the porosity distribution aligns with the size and orientation of dune features observed in the analog 3D seismic data.

No facies model was used to control the porosity petrophysical model. The well control across the model domain is sufficient to effectively estimate porosity using geostatistical methods.

Analysis of proprietary 3D seismic outside of the AoR images a Lyons dune with a length of 20,000 ft, width of 8,000 ft, and orientation of -66 degrees from north. This orientation is consistent with the dominant cross-stratification direction observed in the Juniper M-1 characterization well and the paleo wind direction described in Sonnenberg (1981), Oldham (1996), and Lee and Bethke (1994).

The porosity property model was generated using an elliptical variogram matching the observed orientation and length-to-width ratio: -66 degrees from north, with a major anisotropy range of 50,000 ft and a minor of 20,000 ft. The ratio of the utilized anisotropy ranges is consistent with seismically imaged dunes, while the magnitudes are large enough to continue to honor offsetting well control in areas without data.

Porosity was distributed in the model using the Gaussian Random Function Simulation algorithm and the elliptical variogram. **Figure 3.16** provides a histogram of the input well log data, upscaled cells, and the resulting property model for the Lyons Formation injection zone. Maps (**Figure 3.14, Figure 3.15**) and cross-sections (**Figure 3.17 and Figure 3.18)** through the AoR showing the property model are also provided.

Figure 3.16—Histogram plot for porosity. Light red columns represent the distribution of PHIE log data. Green columns represent data distribution of PHIE data once logs have been upscaled into the model grid. Purple/blue columns represent the distribution of the final modeled PHIE property. The histogram shows consistency in PHIE distribution of all three properties, indicating that the final model property output honors the input data.

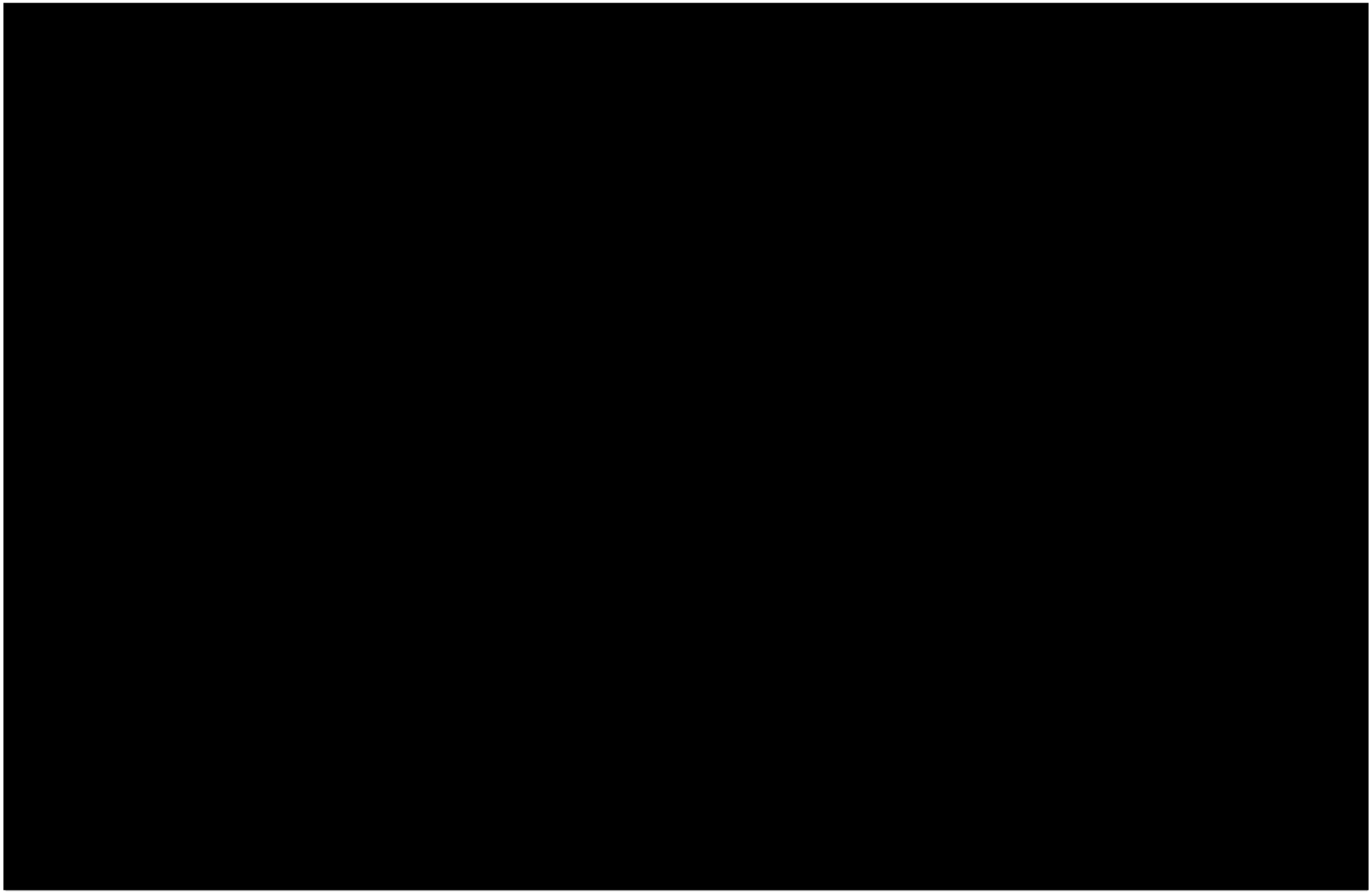

Figure 3.17—Strike-oriented cross-section view of the PHIE modeled property distribution across the AoR, trending N-S. Porosity was modeled in the Goose Egg, Lyons, and Satanka formations.

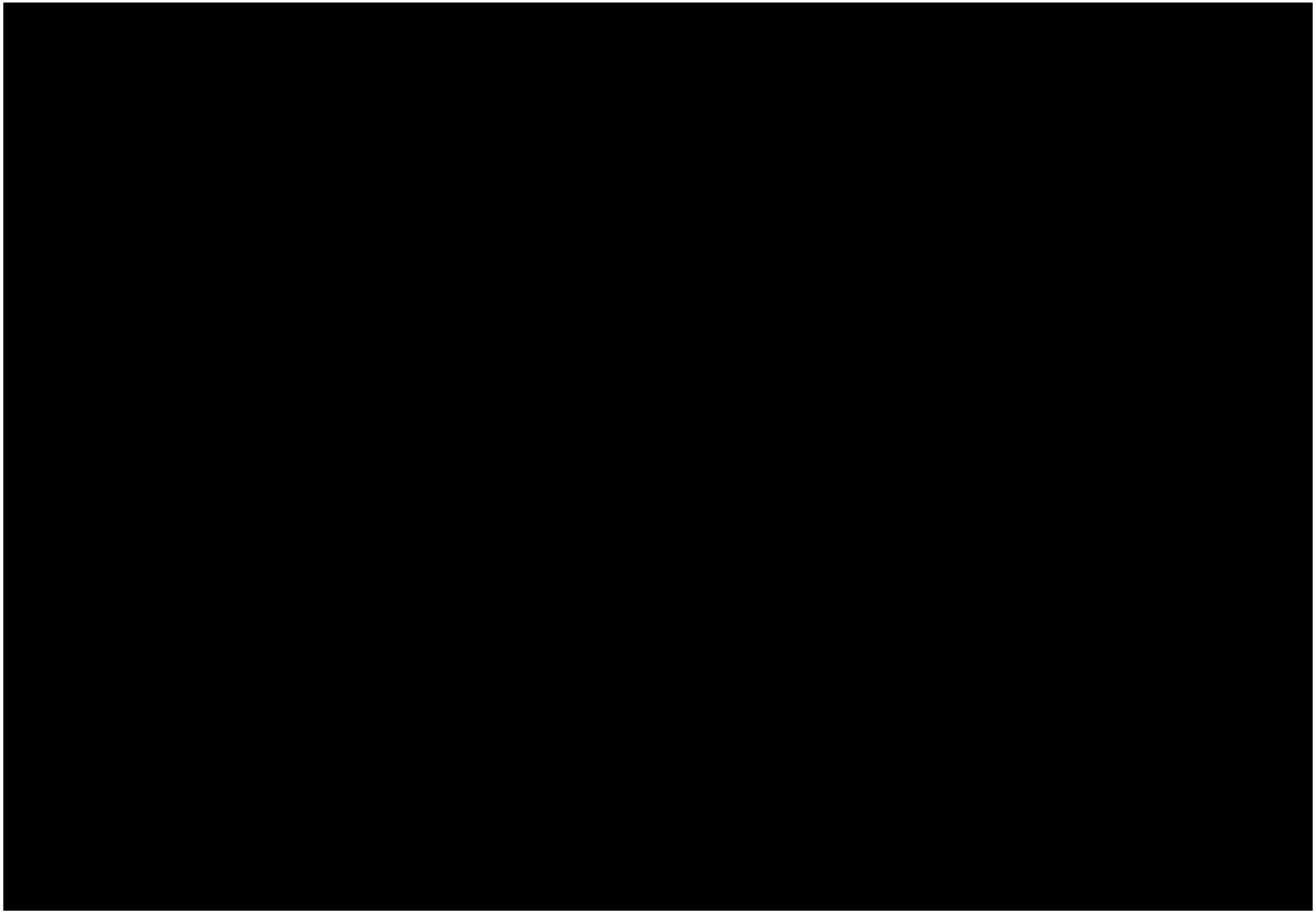

Figure 3.18—Dip-oriented cross-section view of the PHIE modeled property distribution across the AoR, trending W-E. Porosity was modeled in the Goose Egg, Lyons, and Satanka formations.

3.1.3.1.4 Matrix Permeability

The porosity-permeability relationship within the Lyons Formation was determined from routine core analysis (RCAL) measurements (n = 42) and core descriptions within the Juniper M-1 well. There are two sand-bearing facies (Facies "A" and a "B") within the Lyons Formation of the Juniper M-1, both of good reservoir quality and present in roughly equal proportions (**Figure 3.19**). Facies B, however, displays a slightly higher permeability trend for a given porosity and has been therefore assigned a different porosity-permeability trend. Comparison of porosity-permeability relationships within both faces with associated XRD data reveals that Facies B contains a higher proportion of potassium feldspar and, as a result, reads as a higher gamma in wireline logs that can be used as a proxy to determine facies assignment (**Figure 3.20**). In the Conestoga area, Facies B is the dominant facies present.

Figure 3.19—Histogram showing the distribution of permeability by facies. Green columns represent the permeability distribution within Lyons Facies A. Light blue columns represent the permeability distribution within Lyons Facies B. Yellow columns represent the permeability distribution for both the Goose Egg and Satanka formations based on the CRA porosity-permeability relationship.

Figure 3.20—Porosity-permeability transforms for each facies.

Separate porosity-permeability relationships for each facies were evaluated to achieve a better correlation with core RCAL and log data. High Plains used discreet porosity and permeability transforms within the Lyons for each of these distinct facies. Because of the log relationship between gamma ray and each respective facies, a GR cutoff was incorporated to govern facies assignment. Facies A transform was assigned to cells with an API greater than [redacted]; Facies B transform was assigned to cells with an API less than or equal to [redacted] (**Figure 3.21 and Figure 3.22)**. The GR log for each well [redacted] wells) was upscaled and modeled using the same variogram inputs and modeling algorithm as the porosity model (**Figure 3.23 and Figure 3.24**). After the GR property was distributed in the model, the facies cutoff was applied to discretize the two. Equations for respective permeability transforms are as follows:

Equation 3.3—Facies A porosity-permeability transform.

$$K_{FaciesA} = \text{[redacted]}$$

Equation 3.4—Facies B porosity-permeability transform.

$$K_{FaciesB} = \text{[redacted]}$$

.

Figure 3.21—Strike-oriented cross-section view of the GR modeled property distribution across the AoR, trending north-south. GR was modeled in the Goose Egg, Lyons, and Satanka formations to establish cutoffs for facies designations.

Figure 3.22—Dip-oriented cross-section view of the GR modeled property distribution across the AoR, trending west to east. GR was modeled in the Goose Egg, Lyons, and Satanka formations to establish cutoffs for facies designations.

Figure 3.23—Strike-oriented cross-section view of the facies distribution across the AoR, trending north-south. Facies were calculated in the Goose Egg, Lyons, and Satanka formations to establish a porosity-permeability relationship at each cell.

Figure 3.24—Dip-oriented cross-section view of the facies distribution across the AoR trending west-east. Facies were calculated in the Goose Egg, Lyons, and Satanka formations to establish a porosity-permeability relationship at each cell.

Strike and dip cross-sections of the calculated combined permeability property are displayed in **Figure 3.25** and **Figure 3.26**.

Within the Goose Egg (upper confining zone) and Satanka (lower confining zone), a third permeability transform was used to establish a relationship between porosity and permeability of tight seal rocks. Crushed Rock Analysis (CRA) is used on tight rock samples to properly clean low permeability samples more effectively than Routine Core Analysis (RCA) can. CRA also eliminates microfractures that could obscure the nano- and low microdarcy permeability ranges in tight mudstones and siltstones. CRA porosity and permeability measurements for samples (n = 40) in the Goose Egg and Satanka from the Juniper M-1 core were used to create a specific permeability transform for tight rocks in the model. This transform is only related to the porosity property and was applied to all cells within the Goose Egg and Satanka to generate a permeability property that best represents tight seal rocks (**Equation 3.5**).

Equation 3.5—Crushed Rock Analysis (CRA) porosity-permeability transform.

$$K_{CRA} = [redacted]$$

The final modeled properties are summarized in **Figure 3.27** at the Conestoga I-1 location. The distribution of porosity and permeability across the model domain is consistent with existing wireline log data at respective well control points. At the Conestoga I-1 location, the modeled average effective porosity is [redacted] and the average permeability is [redacted] mD

Figure 3.25—Strike-oriented cross-section view of the modeled permeability distribution across the AoR, trending north-south. Permeability was modeled in the Goose Egg, Lyons, and Satanka formations.

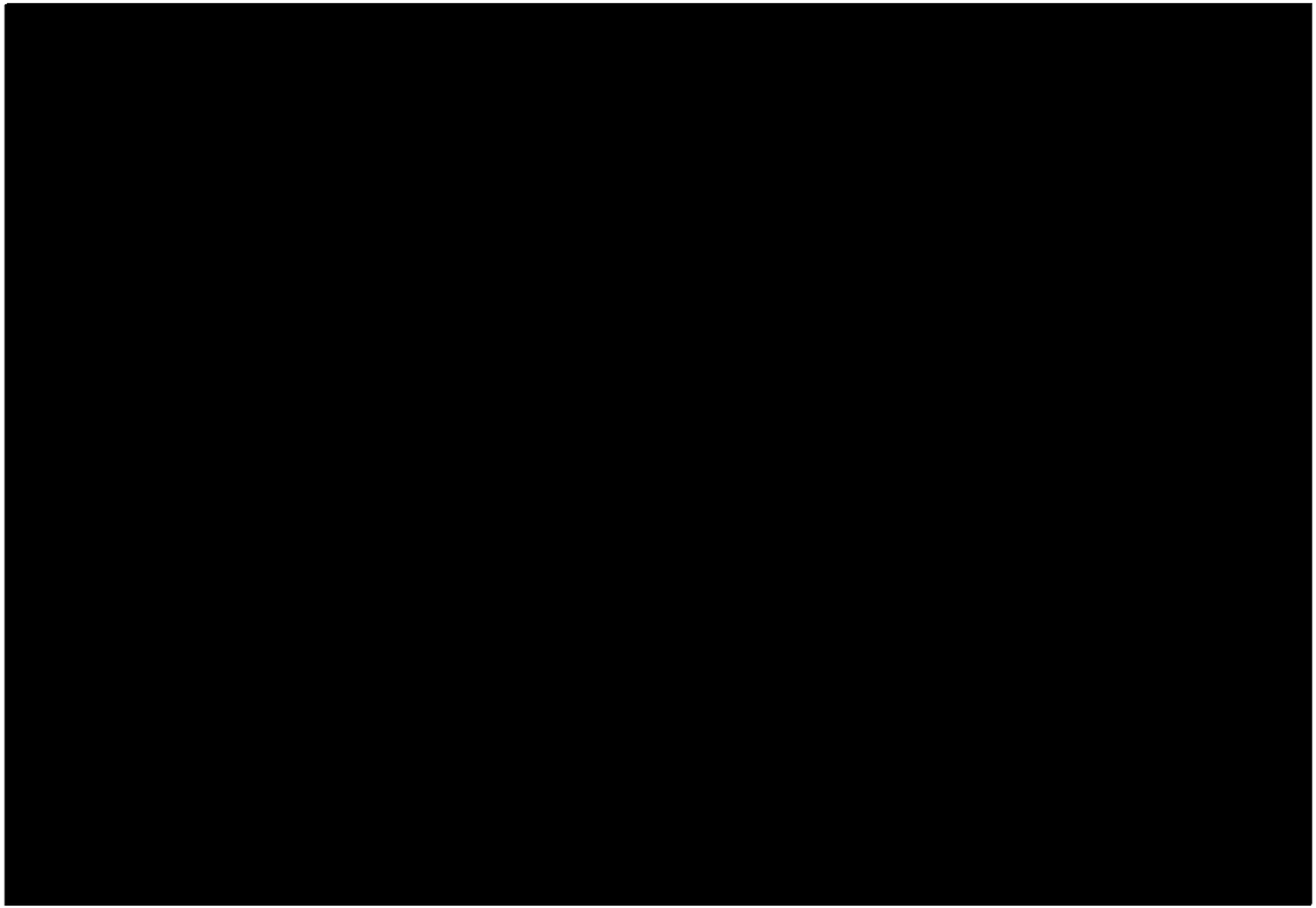

Figure 3.26—Dip-oriented cross-section view of the modeled permeability distribution across the AoR, trending W-E. Permeability was modeled in the Goose Egg, Lyons, and Satanka formations.

Figure 3.27—Raw log data compared to upscaled and modeled properties for the Mathewson 1 type-well and modeled properties expected at the Conestoga I-1 location. The “Gamma Ray” track displays the gamma ray from log data, increasing from 0 to 150 API from left to right. “GR [Modeled]” is the gamma ray property generated in the petrophysical model, increasing from 0 to 150 API from left to right. The “Porosity” track displays the PHIE from log data, increasing from 0 to 30% API from right to left. “POR [Modeled]” is the PHIE property generated in the petrophysical model, increasing from 0 to 30% from right to left. The “Facies” track displays the facies designation for permeability transform based on the associated GR [modeled] cutoff. Pink is Facies A, blue is Facies B, and green is CRA used in the upper and lower confining zones. The furthest column on the right, “K [Modeled],” is the resulting modeled permeability property, increasing from 0.001 mD to 10,000 mD from right to left. Changes in the modeled permeability property are displayed in the distance between the two wells.

3.1.3.2 Potential for Future Updates

The static geologic model and the dynamic reservoir simulation represent a baseline that will be compared with future data and updated with new well data, including core analysis, log interpretations, and operational measurements and testing results. Each measurement will be systematically incorporated to refine future models, with every change in outcome compared to the original or subsequent models to quantify incremental changes across the Project area. Critical parameters to be obtained from the Conestoga I-1, including permeability, porosity, thickness, and injectivity, will be used to update the model as necessary. The model will be history-matched to the recorded injection pressures, volumes, and rate of plume growth to further tune input parameters. Following each iteration, changes in the pressure regime, potential pressure front (if generated), and plume size will be compared to the original boundaries of the AoR and adjusted accordingly.

High Plains plans to acquire whole conventional cores from the Lyons Formation within the AoR. The acquisition, interpretation, and laboratory analysis of these cores will enhance the understanding of the reservoir at the injection site and contribute to a more robust geomodel. This will include more data on the distribution of each facies and the porosity-permeability relationships within the Conestoga I-1's AoR.

The structural interpretation and facies model will be refined by integrating additional seismic interpretations from licensed 2D surveys. Incorporating site-specific core data and seismic attributes within the AoR will provide the necessary inputs to conduct uncertainty analyses on various static and dynamic model parameters.

3.1.3.3 Dynamic Model Geometry

The static geologic model was used as input for the dynamic reservoir simulation. To reduce the run time of the dynamic simulation, the regional static geomodel was cropped to a smaller domain (**Figure 3.12**). The dynamic model domain covers an area of 5,900 sq miles and consists of 14,760,739 3D grid cells arranged in a 551×301×89 (I×J×K) grid configuration. The grid size is 1,000×1,000 ft. All horizons, layering, and properties remained unchanged following cropping.

The CO_2 injector well, Conestoga I-1, was included in the model to develop the plume and pressure responses. **Figure 3.28** shows a 3D fence diagram of the dynamic grid with the permeability property and the injection well shown. The base of the injection zone (top lower confining zone, Top Satanka Formation) is displayed in green. Domain information for the dynamic grid is summarized in **Table 3.1**.

Figure 3.28—3D view representation of the dynamic reservoir model with the permeability property and showing the location of the injection well. The top Satanka surface (base injection zone) is displayed as the lower bounds, with the permeability property for the Lyons overlain as a fence grid.

Table 3.1—Model domain information for the dynamic grid.

Coordinate System	NAD83 BLM Zone 13N
Horizontal	NAD 83
Coordinate System Units	US ft
Zone	BLM 13N
FIPSZONE	
Coordinate of X min (ft)	
Coordinate of Y min (ft)	
Elevation of top of domain (ft, TVDSS)	

* Grid centroids in CMG™ Builder

3.1.4 Permeability

Permeability is a crucial subsurface parameter impacting the rate of fluid flow and the resulting injection pressure. Permeability is related to changes in porosity, pore size, and pore structure. Permeability values were provided from the static model, distributed using the data and methodology described in *Section 3.1.3.1*. The dynamic model used a vertical-to-horizontal permeability ratio (kv/kh) of 0.05.

3.1.5 Constitutive Relationships and Other Rock Properties

3.1.5.1 Relative Permeability and Capillary Pressure

The model incorporated two sets of relative permeability curves, one to represent the supercritical CO_2-rich ("gas") phase[1] and another to represent the aqueous ("water") phase. These curves were entered into the model as functions of phase saturations. Two tables were used: one for the sandstone lithologies of the Lyons Formation and another for the confining zones. The sandstone

curve represented relative permeability measurements from five Lyons sand samples collected at different depths in the Juniper M-1 well. The relative permeability data for the confining zones were based on datasets from Bennion and Bachu (2007). Drainage relative permeability curves were used, assuming a non-wetting CO_2-rich phase displacing the wetting phase, the formation brine.

Relative permeability and capillary pressure curves (**Figure 3.29**) were generated from representative core samples collected in the Lyons Formation from the Juniper M-1 well, using Special Core Analysis (SCAL) (sampled at 9,152 ft MD) and Mercury Injection Capillary Pressure (MICP) (sampled at 9,148 ft MD). The relative permeability curves for the target storage formation were assumed to behave similarly to sandstone members from the Juniper M-1 well. The gas-trapping effect on relative permeability hysteresis was modeled with a residual gas saturation of 0.3, consistent with experimental values from Bennion and Bachu (2008). Relative permeability curves for the upper and lower confining zones were modeled using data from Bennion and Bachu (2007) for shale-type rocks to low-permeability anhydrite/shale.

Figure 3.29—Relative permeability and capillary pressure curves. (a) supercritical CO_2-water relative permeability curves; (b) capillary pressure for the Lyons Formation.

3.1.5.2 Pore Pressure

The pore pressure was analyzed using wireline logs from the nearest (miles southeast) offsetting Lyons penetration, (see *Section 2.6* for more details). Pore pressure is a critical input parameter for the dynamic simulation model and directly affects the size of the plume and the CO_2 volume injected. The model assumed an initial pressure of psi at a datum depth of

3.1.5.3 Fluid Properties

The salinity of the Lyons Formation brine was assumed to be mg/L, resulting in a dynamic viscosity of centipoise (cP). The dynamic simulation estimated a brine density of lbm/ft^3

for the Lyons. No direct fluid samples are available from within the AoR. These values will be updated pending laboratory analysis of future fluid samples.

The gas stream composition of the injected gas was modeled for the Conestoga I-1 well using a minimum of 95% CO_2 with small to trace quantities of other components, including less than 5% nitrogen, oxygen, hydrogen sulfide, hydrogen, water, and hydrocarbons. For computational efficiency, only the most representative components in the gas stream with higher concentrations were included in the model. The injected gas composition included in the dynamic reservoir model comprised [redacted].

The fluid model was conducted with the Peng and Robinson (1976) equation of state (EOS) to estimate fluid properties of the CO_2-supercritical phase (**Figure 3.30)**. CO_2 saturation properties calculated from the EOS were in good agreement with experimental data obtained from the U.S. Department of Commerce's National Institute of Standards and Technology (NIST) Chemistry WebBook database (NIST, 2024).

For the aqueous phase, the simulator estimated the density using the Rowe-Chou correlation (CMG-GEM™), while viscosity was estimated using tables from experimental measurements of aqueous solutions following Kestin et al. (1981). The solubility in the aqueous phase was modeled by the general expression of Henry's Law, considering the effect of both pressure and temperature (Harvey, 1996).

Without site-specific datasets, fundamental fluid properties were defined using default values in the CMG's GEM WINPROP™ components database. WINPROP™ is CMG's fluid property characterization tool (CMG's WINPROP User Manual, 2024).

Figure 3.30—Pressure-temperature diagram.

3.1.5.4 Rock Compressibility

Rock grains in the reservoir experience external stress from the accumulation of overburden and pore pressure from fluids in the pore space. Rock compressibility (C_r) quantifies the change in rock volume because of these forces. Isothermal rock compressibility was assumed to be 3.43 × 10^{-6} 1/psi, within the typical range of sandstones calculated using Hall's (1953) equation (**Equation 3.6)**. An assumed porosity (φ) of [redacted] v/v from the core sample used for SCAL evaluations (at 9,152 ft) was applied uniformly throughout the model. This value aligns with bulk compressibility measurements on a Lyons Sandstone sample from the Juniper M-1[redacted]

Equation 3.6—Hall's (1953) correlation.

$$C_r = 1.87 \times 10^{-6} \times \varphi^{-0.415} \; [1/psi]$$

Where:

C_r = total compressibility of reservoir rock [1/psi]
φ = porosity [v/v]

3.1.6 Boundary Conditions

The reservoir was assumed to be semi-closed and fully saturated with brine. The aquifer boundary conditions were assumed to be open (infinite aquifer), acting over the horizontal boundaries at the south, west, and east. However, the north side of the model was assumed to be a closed boundary to represent the approximate location where the Lyons Formation sandstone facies grade into evaporites of the time-equivalent Stone Corral Formation. To simulate a semi-closed system, the pore volume at the model's edge was adjusted with a pore volume multiplier (MULTPV), where the pore volume of edge cells is set to be 10,000 times larger than the volume implied from the static model. **Figure 3.31** illustrates the open boundary conditions (red grid blocks) at the model's east, south, and west edges. No flow boundary conditions were applied in the vertical direction at the upper and lower faces of the model.

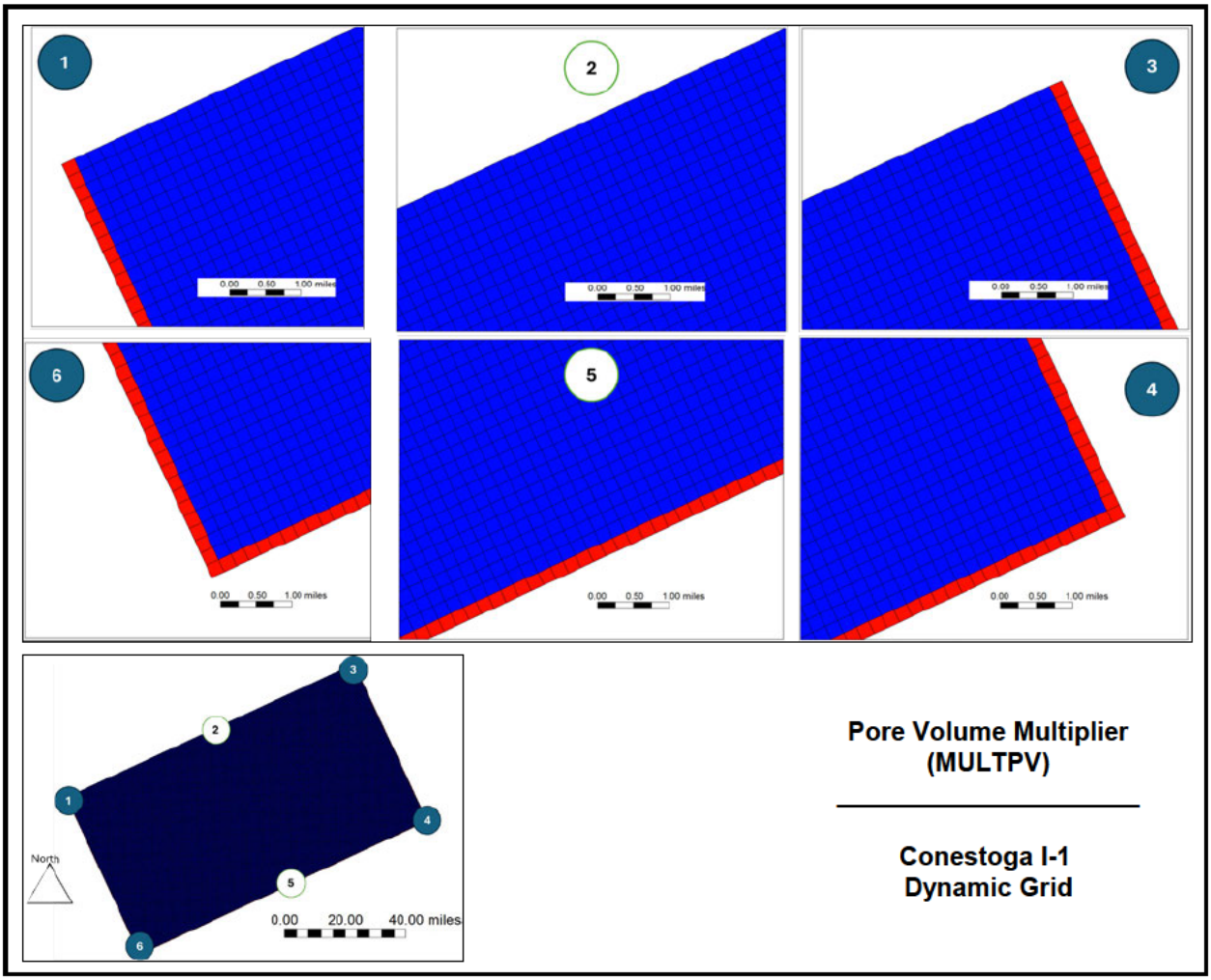

Figure 3.31—Pore volume multiplier (MULTPV) map used to simulate a semi-closed boundary condition. The upper frame is zoomed into each point: top-left corner (1), bottom-left corner (6), mid-top face (2), mid-bottom face (5), top-right corner (3), and bottom-right corner (4). Blue-colored cells represent MULTPV = 1; red-colored cells represent MULTPV = 10,000.

3.1.7 *Initial Conditions*

Pore pressure, temperature, and brine salinity were used to initialize the model. Initial pressure was calculated using the vertical equilibrium option in CMG-GEM™ and saturations from the capillary pressure tables. There was no transition zone, as the initial water-gas contact was set above the lowest model elevation. The initial pressure was calculated using a hydrostatic pore pressure gradient of 0.443 psi/ft. The initial temperature was calculated using a temperature gradient of [redacted] °F/ft, resulting in an initial pressure of [redacted] psi and a temperature of [redacted] F at a modeled datum depth of [redacted] (**Table 3.2**). The model assumed that the initial reservoir pressure is in hydrostatic equilibrium.

The target formation was saturated with brine at an initial [redacted] mg/L concentration. The initial water phase density was calculated using the Rowe-Chou correlation within the CMG-GEM™ simulator based on the initial pressure and temperature values. No oil phase was specified in the injection zone; however, a trace component with a small molar fraction, in the order of 10^{-5}, of one hydrocarbon component (methane) was dissolved in the brine. This parameter choice was based

on CMG™'s recommendations to improve solver stability during the fugacity calculations for CO_2 simulations in deep saline aquifers.

Table 3.2—Dynamic reservoir model initial conditions.

Parameter	Value or Range	Units	Data Source
Average Reservoir Permeability* (Lyons)	[redacted]		
Average Reservoir Porosity* (Lyons)			
Reservoir Pore Pressure Gradient			
Max Bottomhole Injection Pressure			
Temperature Gradient			
Initial Reservoir Temperature**			
CO_2 Phase			
Salinity (TDS)***			
Fluid Density**			
Brine Viscosity**			
Rock Compressibility			

* Pore volume weighted average.
** Evaluated at initial conditions at the top perforation ([redacted]
*** The dynamic model represents salinity in terms of an equivalent sodium chloride (NaCl) salinity.

3.1.8 Operational Information

Details of the injection operation proposed for the Conestoga I-1 injection well are presented in **Table 3.3**. It shows the estimated bottomhole pressure (BHP) and wellhead pressure (WHP) from the dynamic simulation outputs. BHP values resulting from the simulation are below the maximum allowable BHP of [redacted] psi calculated using 90% of the estimated fracture gradient ([redacted] psi/ft) at the top perforation of the well. WHP is constant during the injection period ([redacted] psi). **Figure 3.32** shows the modeled BHP and WHP over time.

Table 3.3—Operating details.

Operating Information	Conestoga I-1
Location (global coordinates)* X (Longitude) Y (Latitude)	[redacted]
Model coordinates (ft) X Y	
No. of perforated intervals	
Perforated interval (ft) Z top Z bottom	
Tubing outer diameter (inches)	
Planned injection period Start End	 01/01/2027 01/01/2039
Injection duration (Years)	12
Average Injection rate (Mta)*	2.26

* NAD83

Figure 3.32—Injection wellhead pressure and bottomhole pressure versus time.

The model assumes that the well operation is constrained either by maximum injection WHP or by maximum BHP. The maximum allowable WHP (psi) was defined in the model by the proposed operational data. As the maximum bottomhole injection pressure did not exceed 90% of the Lyons Formation fracture pressure, the injection rate was controlled by the maximum WHP.

The wellbore modeling feature from CMG-GEM™ was used in the dynamic model to specify the surface-to-reservoir wellbore pressure drop. Pressure drop was computed from a hydraulics table developed using the industry standard software Petroleum Experts PROSPER™ (PROSPER Manual, 2024). Hydraulic tables were calculated with inputs from wellbore design parameters for a -in. (outside diameter) tubing size, wellbore length, and a wellhead temperature of °F.

Figure 3.33 presents the mass injection rate in millions of metric tons per annum (Mta) and the cumulative mass injected in millions of metric tons (Mt) from the model. The cumulative CO_2 mass for 12 years of injection resulted in 27.1 Mt with an average injection rate of 2.26 Mta. These results are also summarized in **Table 3.4** for the 12 year of injection and 50-year post-injection periods.

Figure 3.33—CO_2 injection mass rate (Mta) and cumulative mass (Mt) for 12 years of injection.

Table 3.4—Tabular data from simulation results.

Year	Bottomhole Injection Pressure (psi)	Wellhead Injection Pressure (psi)	CO_2 Mass Injection Rate (Mta)	Cumulative CO_2 Injected (Mt)
2027	[redacted]			
2028				
2029				
2030				
2031				
2032				
2033				
2034				
2035				
2036				
2037				
2038				
2039				
2040				
2041				
2042				
2043				
2044				
2045				
2046				
2047				
2048				
2049				
2050				
2051				
2052				
2053				
2054				
2055				
2056				
2057				
2058				
2059				
2060				
2061				
2062				
2063				
2064				
2065				

Year	Bottomhole Injection Pressure (psi)	Wellhead Injection Pressure (psi)	CO_2 Mass Injection Rate (Mta)	Cumulative CO_2 Injected (Mt)
2066	[redacted]			
2067				
2068				
2069				
2070				
2071				
2072				
2073				
2074				
2075				
2076				
2077				
2078				
2079				
2080				
2080				
2081				
2082				
2083				
2084				
2085				
2086				
2087				
2088				
2089				

3.1.9 Fracture Pressure and Fracture Gradient

No injection tests have been conducted within the AoR; therefore, the model relied on characterization data from offset wells. The fracture gradient in the Lyons for the Conestoga I-1 well was estimated to be [redacted] psi/ft (further detailed in *Section 2.6*). The fracture gradient will be updated as High Plains acquires additional data to better constrain this value (e.g., injectivity test, mini-fracs). The maximum allowable BHP set in the dynamic model was 90% of the estimated fracture gradient at the top perforation of the well. Based on this calculation, the maximum injection pressure at the top of the perforated interval was [redacted] psi. These values are listed in **Table 3.5**.

Table 3.5—Injection pressure details.

Injection Pressure Details	Value
Fracture pressure gradient (psi/ft)	[redacted]
Maximum injection pressure (90% of fracture pressure gradient) (psi)	
Elevation corresponding to maximum injection pressure (ft, TVD)	

3.2 Computational Modeling Results

3.2.1 Predictions of System Behavior

The simulation described in this document was conducted primarily to calculate the reservoir's storage capacity, delineate the future plume size and position, assess pressure changes and the resulting pressure front, and determine the Area of Review. Predictions of system behavior were developed following the EPA guidance regarding modeling requirements and recommendations for delineating the AoR (*Underground Injection Control Program Class VI Well Area of Review Evaluation and Corrective Guidance for Owners and Operators*). All simulations were performed with CMG-GEM™ v2024.10. Several iterations of model testing were conducted prior to running the model to ensure that grid spacing and boundary conditions did not result in numerical artifacts negatively impacting the results.

3.2.1.1 *Storage Capacity Estimation*

The results of the simulation indicate that, under the injection operation conditions evaluated, the Conestoga I-1 is capable of injecting 27.1 Mt during the 12-year injection period at an average injection rate of 2.26 Mta (**Table 3.4, Figure 3.33)**. BHP values from the simulation were below the maximum allowable injection pressure target, and the injection well was controlled by the WHP of [redacted] psi constraint, as shown in **Figure 3.32**.

As detailed in *Section 2.10.2.1*, the storage capacity of the Lyons Formation within a two-mile radius is conservatively estimated at 54 Mt, based on assumptions of [redacted] porosity, [redacted] irreducible water saturation, and an efficiency factor of 50%. This estimate is twice the planned injection mass of 27.1 Mt. It is important to note that this storage capacity calculation assumes the entire reservoir height is utilized for CO_2 storage. However, this is generally not the case due to buoyancy effects, which are not accounted for in the calculation but are considered in the simulation. This buoyancy effect largely explains the difference between the AoR radius and the storage capacity estimate.

3.2.1.2 *Trapping Mechanisms*

Four trapping mechanisms act on geologically sequestered CO_2. First, hydrodynamic trapping, or structural trapping, is a physical trapping mechanism where a sealing rock or structural trap halts CO_2 migration. Second, residual CO_2 trapping is another physical mechanism where the imbibition of brine traps CO_2. Third, solubility trapping is a chemical trapping mechanism where CO_2 dissolves into the formation fluid, forming a CO_2-enriched brine. Fourth, mineralization is another form of chemical trapping that forms limestone from geochemical reactions of CO_2 and the rock. Hydrodynamic and residual CO_2 trapping are expected to be the primary near-term mechanisms for containing the CO_2 injected as part of the Project. Solubility and mineralization will play a

secondary role but will take hundreds of years to affect the plume. These four mechanisms are detailed further as follows.

Hydrodynamic Trapping

Hydrodynamic trapping is a physical form of trapping in which injected CO_2 migrates upwards until it encounters an impermeable cap rock. CO_2 is less dense than formation brine and will continue to travel due to buoyant forces. CO_2 will cease moving once it reaches a confining zone with higher capillary entry pressure than the hydrodynamic force (Zhang and Song, 2014). Pinch-outs or facies changes of the injection zone may act as structural traps to prevent CO_2 migration. The injectate will then accumulate under this trap, similar to a gas cap seen in natural gas reservoirs.

Residual CO_2 Trapping

Residual trapping is another physical form of trapping CO_2 within the pore space caused by brine imbibition after the injected fluid displaces the brine. In a brine-filled reservoir, the grains of the rock are naturally water-wet (Juanes et al., 2006). During injection, the nonwetting fluid (i.e., supercritical CO_2) will first displace the brine, otherwise known as drainage. After injection ceases, the plume will continue to migrate upwards; as it does, the wetting fluid (i.e., brine) will reenter the pore space below, displace some nonwetting fluid, and trap the rest (Zhang and Song, 2014). This displacement of the nonwetting fluid due to the wetting fluid is known as imbibition.

Solubility Trapping

Solubility trapping is a chemical form of trapping where the supercritical CO_2 dissolves in the formation brine. CO_2 will come into contact with the formation brine as the plume travels. CO_2 is highly soluble in the brine, resulting in a denser solution and thus allowing it to sink to the bottom of the reservoir. The solubility of CO_2 in water is a function of temperature, pressure, and water salinity (Chang et al., 1998). Higher salinities and temperatures make it more difficult for the CO_2 to dissolve in brine. However, higher pressures will allow more CO_2 to dissolve. This process occurs on the timescale of hundreds of years.

Mineralization

Also known as mineral trapping, mineralization is a process that occurs over hundreds of years. This form of chemical trapping occurs when the injected CO_2 reacts with the reservoir rock and brine, dissolving in the saline water and forming a weak carbonic acid. The acid then reacts with the rock to form a solid carbonate mineral and becomes immobile. A variety of chemical reactions have been documented.

The model does not incorporate mineralization, potentially increasing the modeled CO_2 plume's lateral extent.

Figure 3.34 shows the estimated contribution of the different trapping mechanisms considered during the injection and post-injection periods. From the simulation results for Conestoga I-1 well, the structural (free-phase CO_2) and residual (capillary) trapping processes were found to be the dominant trapping mechanisms during the forecast period. CO_2 dissolution into the aqueous phase also contributes significantly to CO_2 storage security.

Figure 3.34—Simulated total free-phase supercritical CO_2, CO_2 trapped (capillary), and CO_2 dissolved in brine.

Most injected CO_2 at the end of the injection period remains stored as free-phase CO_2. The capillary trapping mechanism can immobilize a portion of this free-phase CO_2 plume in the pore space during the post-injection period. Capillary forces are represented in the model by the relative permeability and capillary pressure inputs.

Both structural and capillary trapping mechanisms could be enhanced by local, primarily vertical, heterogeneities that provide barriers to buoyancy-driven flow.

The trapping mechanism results in **Figure 3.34** show that significant amounts of CO_2 can be dissolved in the formation brine. A decrease in the free-phase CO_2 is an effect of the rate of CO_2 dissolution in brine and the CO_2 trapped during the post-injection period. Simultaneously, the dissolution and capillary trapping mechanisms continue to increase post-injection, lowering the migration risk.

3.2.1.3 *CO_2 Migration*

CO_2 migration in the reservoir was calculated from the simulation. **Figure 3.35** shows a west-to-east cross-section through the injection well, displaying the modeled free-phase CO_2 saturation. Two snapshots are shown, one at the end of the injection (EOI) and another at the end of the post-injection period, corresponding to the end of the 50-year PISC (2089). CO_2 plume boundaries are shown for each snapshot. After the EOI, the CO_2 plume continues to expand in the Lyon

Formation, primarily up-dip (east). The results show the CO_2 plume is contained inside the target storage formation. The sealing capacity of the fine-grained upper caprock constitutes an effective means to stop vertical migration.

Figure 3.36 shows a map with a time-lapse of the modeled CO_2 plume extents from 2039 to 2089. The final stabilized CO_2 plume boundary is approximately [redacted] ft. CO_2 plume stabilization was estimated based on the change of CO_2 plume radius with time, as shown in **Figure 3.37**.

As the model does not consider geochemical reactions (mineralization), the free-phase CO_2 saturation CMG-GEM™ output was taken as a proxy for supercritical CO_2 concentration.

The lateral migration of the CO_2 plume is mainly caused by buoyancy, with the CO_2 rising to the top of the injection zone, reaching the lower permeability layers at the base of the upper confining zone, and then moving outward along this interface. This is demonstrated in the cross-section through the plume at the end of PISC (**Figure 3.35b)**. The CO_2 concentration is highest at the center of the plume and near the well at the end of the injection period (**Figure 3.35a**) then it gradually disperses toward the plume's edges, where CO_2 saturation is lower.

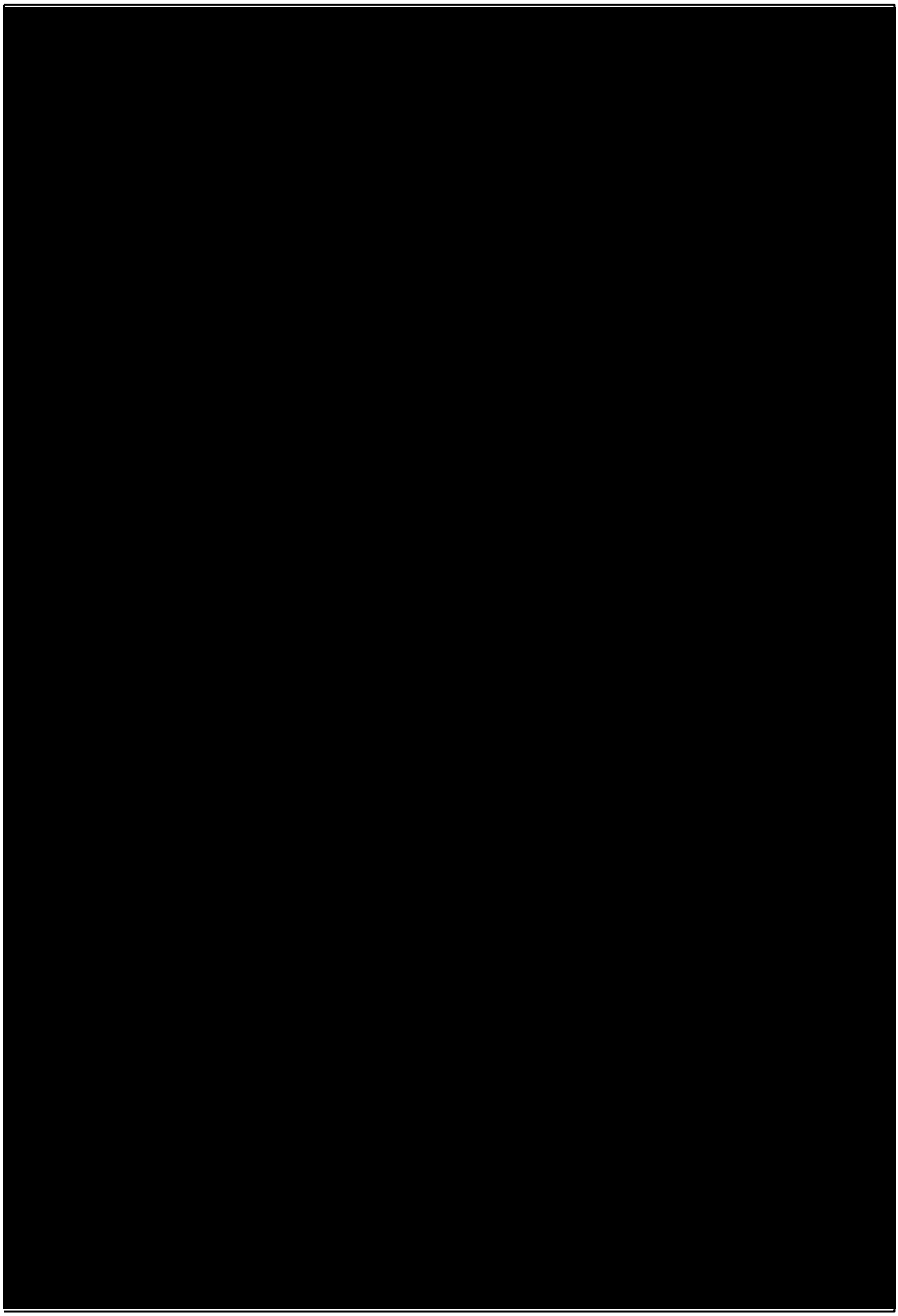

Figure 3.35—Cross sections showing CO_2 concentration at (a) the end of injection and (b) at the end of the 50-year post-injection site care (PISC) period displayed west-to-east through the Conestoga I-1 well; (c) plume boundaries at the end of the injection period in year 2039 (EOI, model year 12), and at the end of the PISC in year 2089 (model year 62, AoR).

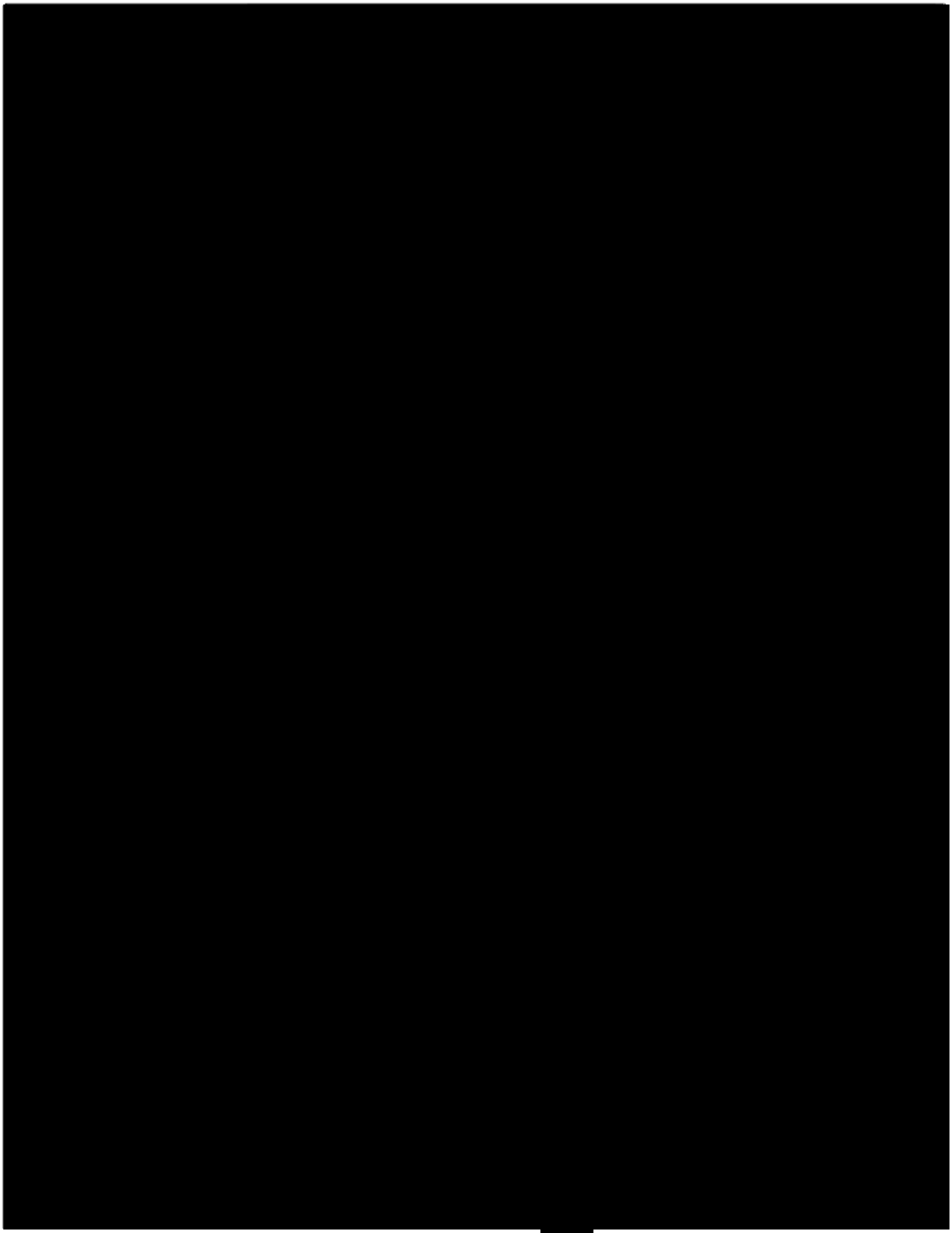

Figure 3.36—Time-lapse of modeled injectate plume extents [redacted] saturation) from 2029 to 2089.

Figure 3.37—Change in plume radius over time. The CO_2 plume radius is considered stable (less than 1% change in plume radius per year) in January 2054, which is 15 years after the end of injection (EOI).

Average Pressure Differential

The average pressure differential in the injection zone at the end of injection (year 2039) is shown in **Figure 3.38** while the average pressure differential at the end of PISC (year 2089) is provided in **Figure 3.39**. Both figures also show the modeled plume extent at their given time-step. The CO_2 plumes are displayed in terms of the free-phase CO_2 saturation with a gas saturation cut-off of

A maximum differential pressure of psi is observed at the top perforation depth of the well ft MD) after the 12-year injection period.

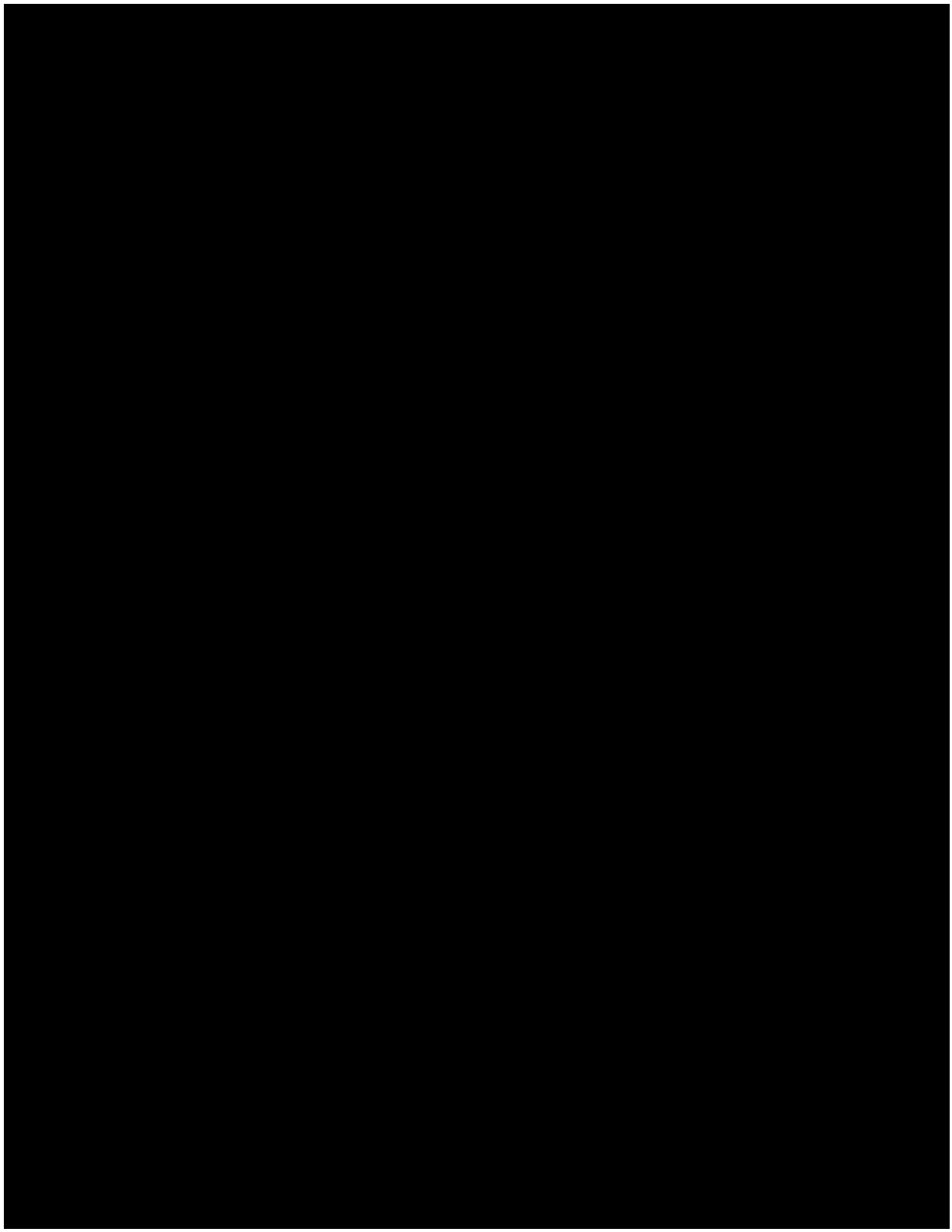

Figure 3.38—Average pressure differential within the Lyons Formation at the end of injection (model year 12). Polygons show areas with [redacted] injectate concentration after 12 years of injection (purple) and 50 years post injection (the AoR; red dashed).

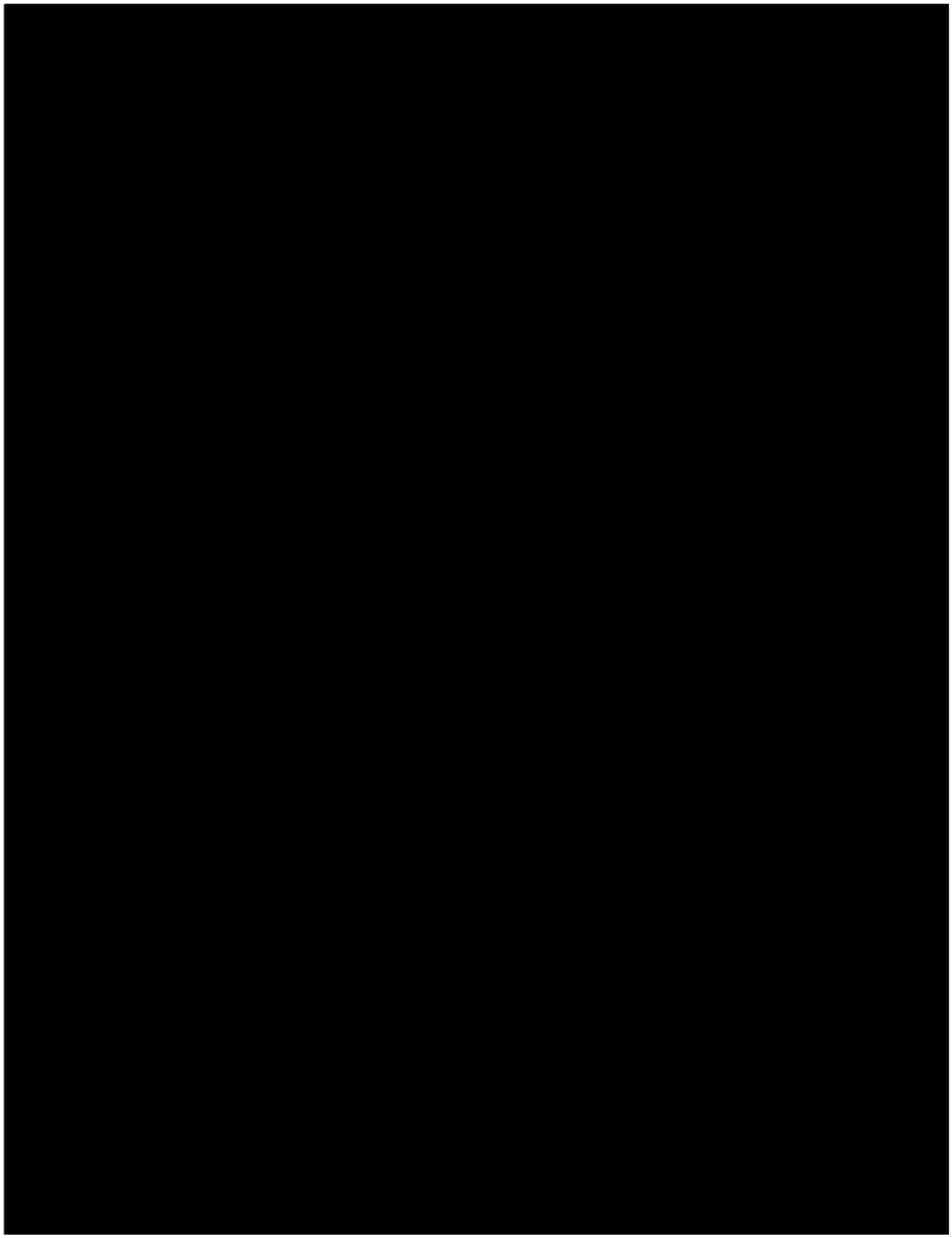

Figure 3.39—Average pressure differential within the Lyons Formation in model year 62 (2089), 50 years post the end of injection, the end of the PISC period. A polygon showing the area with [redacted] gas saturation in model year 62 (the AoR) is shown in red.

Plume Stabilization

Figure 3.37 shows the annualized change in CO_2 plume radius over time. Results show that the plume radius changed significantly during the injection period from January 2027 to January 2029. From the end of injection (EOI, January 2039) until 15 years after EOI (January 2054), the plume radius change decays gradually. The change in plume radius is observed to be stabilized (< 1% increase per year) 15 years after the end of injection.

3.2.1.1 *Potential for Future Updates*

The principal source of uncertainty identified during the modeling and simulation process is the lack of direct, site-specific, measurements to calibrate the model. As additional data is collected, the model's input parameters will be adjusted, and the simulations will be re-run using the collected datasets to reduce model uncertainty. These new parameters will establish a baseline from which injection rate and pressure data collected at the injection well will be used to history-match the model to the observed data. This history match further tunes the laboratory measurements to account for variability in the subsurface parameters that cannot be directly measured and quantified.

3.2.1.2 Model Calibration and Validation

As the model is iterated with data from the injection and monitoring wells, sensitivity analyses will be incorporated into the model documentation. Once injection commences, history matching will be performed and incorporated into AoR re-evaluations.

3.3 Area of Review Delineation

3.3.1 Critical Pressure Calculations

The methodology for calculating critical (also referred to as 'threshold') pressure has been calculated following the *U.S. Environmental Protection Agency's (EPA) Underground Injection Control (UIC) Program Class VI Well Area of Review Evaluation and Corrective Action Guidance*. Calculations assume a hypothetical scenario of a conduit open to both the injection zone and the lowermost USDW.

The depth of the base of the lowermost USDW, as discussed in *Section 3.1.2,* is approximately [redacted] ft below ground surface (bgs), as determined from offset logs. The critical pressure is calculated for the top of the proposed well perforation in the injection zone, estimated at [redacted] ft TVD. The fluid in the injection zone is assumed to be brine with a [redacted] mg/L TDS concentration and a pore pressure gradient of [redacted] psi/ft. A summary of the calculation inputs is included in **Table 3.6**.

Table 3.6—Input values for critical pressure calculation.

Input	Value
Depth to Base of USDW (ft, TVD)	[redacted]
Depth to Top of Injection Zone (ft, TVD)	
Temp. in USDW (°F)	
Temp. in Injection Zone (°F)	
Salinity in USDW (mg/L)	
Salinity in Injection Zone (mg/L)	
Fluid Density in USDW (lbm/ft^3)	
Fluid Density in Injection Zone (lbm/ft^3)	
Initial Pressure at Base of USDW (psi)	
Initial Pressure at Top of Injection Zone (psi)	

The calculations for the critical pressure differential (ΔP_c) and the description of each term is provided in **Equation 3.7**. If $\Delta P_c = 0$, the reservoir and the USDW are in hydrostatic equilibrium. If $\Delta P_c > 0$, the reservoir is underpressurized relative to the USDW. If $\Delta P_c < 0$, the reservoir is over-pressured relative to the USDW.

Equation 3.7—Calculation for the critical pressure differential.

$$\Delta P_c = P_{USDW} + (dz_i - dz_{usdw}) \times SG_i \times 0.433 \ - P_i$$

Where:

P_{USDW} = Hydrostatic pressure at the base USDW (psi)
dz_i = Depth of the top of the injection zone (ft)
dz_{USDW} = Depth of the base of the USDW (ft)
SG_i = Specific Gravity of the liquid in the injection zone (unitless)
P_i = Hydrostatic pressure at the top of the injection zone (psi)

After the substitution of the input values included in **Table 3.6**, the critical pressure is calculated:

$\Delta P_c =$ [redacted]

$\Delta P_c =$ [redacted]

The calculated critical pressure differential is [redacted] psi. A positive value of ΔP_c corresponds to an injection zone that can accommodate an increase in pressure prior to potential fluid migration through a hypothetical conduit open in the injection zone and the USDW.

3.3.2 Area of Review Delineation

The sequestration Project will generate a plume with high concentrations of CO_2 in the reservoir as well as an area where formation pressure is elevated above initial conditions. For most projects, this area of pressure influence is larger than the CO_2 plume extent. A pressure front, however, is where a "pressure differential is sufficient to cause the movement of injected fluids or formation fluids into a USDW" (40 CFR §146.81(d)). In most cases, this is the minimum pressure needed to cause reservoir fluids to migrate from the injection zone to the USDW through a hypothetical conduit open in both zones (the critical pressure). As injection zone reservoir pressure is never

modeled to exceed critical pressure differential (see *Section 3.3.1*, **Figure 3.38**), no pressure front is generated. Therefore, the AoR for this Project has been determined only to include areas where elevated CO_2 saturations [redacted] in the injection reservoir will occur, the stabilized plume extent.

3.4 Corrective Action

3.4.1 Tabulation of Wells Within the Area of Review

3.4.1.1 Wells Within the Area of Review

All artificial penetrations have been evaluated, including oil and gas wells, water disposal wells, stratigraphic boreholes, plugged and abandoned wells, and water wells within the AoR found in private and state databases. A map depicting all artificial penetrations within and around the AoR is provided in **2.2.1a_HighPlains_Conestoga_1_AoR_Map_Arch_D_1-20k_land-topo.pdf.** A larger scale version (1:16,000) showing recent satellite imagery is provided in **2.2.1b_HighPlains_Conestoga_1_AoR_Map_ArchE_1-16k_SatImage.pdf**. The methods and data sources reviewed are described below.

Oil and Gas Wells

Oil and gas well locations were obtained from the S&P Global Enerdeq well database[2] and cross-referenced for accuracy against the latest version of the Nebraska Oil and Gas Conservation Commission (NOGCC) Nebraska Well Database,[3] dated April 19, 2024. Available well files from the NOGCC were downloaded and reviewed for each identified well to confirm the total depth and zones penetrated. The search revealed that only one of the 189 wells within the AoR penetrates the Lyons Formation injection zone or the Goose Egg Formation upper confining zone: the Mathewson 1 (API No. 26-105-22372).

At High Plains' request, the NOGCC searched their records to verify that no other wells, not in the online database, have been drilled within the AoR. They confirmed that, aside from the [redacted] none of the wells in the AoR were drilled to a depth exceeding [redacted] TVD—the approximate depth to the top of the upper confining zone. The NOGCC's confirmation email, verifying that the Mathewson 1 is the only well within the AoR that has reached the depth of the Goose Egg upper confining zone, is included: **3.4.1a_NOGCC_Email_regarding-Mathewson-1_26105223720000.pdf**.

Additionally, a review of recent satellite imagery within the AoR revealed no evidence of well pads without corresponding wellhead locations in the databases.

A list of all wells within the AoR, indicating the total depth of the well and the deepest formation penetrated, is provided in **Appendix 3.2** and the following file: **3.4.1b_AoR Oil and Gas Well List (S&P Enerdeq)-dist.xlsx.**

[2] https://www.spglobal.com/commodityinsights/en/ci/products/oil-gas-tools-enerdeq-browser.html - Accessed 7/29/2024
[3] http://nogcc.ne.gov/Publications/NebraskaWellData.zip - Accessed 7/29/2024

All publicly available well files and logs from the NOGCC for wells within the AoR are provided in the following file: **3.4.1c_Oil and Gas Well Files_AoR_NOGCC_.zip.**

Water Wells

Water well locations were obtained from the Nebraska Registered Wells Inventory.[4] The records in this database are sourced from the Nebraska Department of Natural Resources. This database was last updated on June 4, 2024. The deepest well within the AoR is drilled to 400 ft bgs. Based on these depths, all are completed in the High Plains Aquifer.

Eight water wells located within the AoR were identified. Six wells are active, one is inactive, and one is decommissioned; four are for livestock watering, three are for irrigation use, and one is for water quality monitoring. A list of water wells within the AoR is provided in **3.4.1b_AoR Water Well List_NE_DNR.xlsx,** and a summary of these wells is provided in **Table 3.7**. Well files for all water wells within the AoR are provided in **3.4.1d_Water Well Files_NE_DNR.zip**.

[4] https://www.nebraskamap.gov/datasets/groundwater-wells-dnr/explore - Accessed 7/26/2024

Table 3.7—Water wells within the Area of Review.

Well ID	DNR Reg No.	Owner	Location (PLSS)	Location (NAD83) (Lat.)	(Lon.)	Completion Date	Depth (ft, bgs)	Status	Use
[redacted]									

3.4.1.2 Wells Penetrating the Confining Zone

One well, Mathewson 1 (API: 26-105-22372), was identified that penetrates the upper confining and injection zones within the AoR. The details for this well are shown in **Table 3.8** below. The Mathewson 1 well currently does not have a cement plug across the upper confining zone. Therefore, High Plains plans to perform corrective action on the Mathewson 1 prior to the start of the Project.

Table 3.8—Well within the Area of Review that penetrates the upper confining and injection zones.

UWI 10	Well Name	Operator	Location (PLSS)	Location (NAD83) (Lat)	(Lon)	Spud Date	Total Depth (ft)	Status	Fm. at TD
[redacted]									

3.4.1.2.1 Corrective Action Plan - [redacted]

The [redacted] was originally abandoned in [redacted] with abandonment plugs across the Cherokee, Wolfcamp, and Huntsman formations. These plugs were placed in the openhole section with no casing or cement plugs across the proposed injection, upper confining, or certain hydrocarbon-bearing intervals. Additional abandonment plugs were placed across the surface casing shoe and at the surface.

As no cement plug was placed across the Goose Egg Formation upper confining zone at the time of initial abandonment, in its current state, the [redacted] could potentially provide a pathway for injection or formation fluids to migrate out of the injection zone. Therefore, High Plains plans to perform corrective action on the [redacted] by placing a remedial acid-resistant cement plug across the injection and upper confining zones and additional cement plugs across overlying hydrocarbon-bearing zones.

Details of the well's current construction and the proposed corrective plan are below.

Critical Markers and Planned Plugs

Table 3.9 provides depths to the key formations penetrated by the Mathewson 1 well.

Table 3.9—Geologic markers for the Mathewson 1.

Wolfcamp (ft)	Goose Egg / Lykins / Lyons / Satanka (ft)	Huntsman / Skull Creek / Dakota / Morrison / Sundance (ft)	Niobrara / Codell (ft)	Shannon (ft)
[redacted]				

Details of the panned depths and volumes of remedial plugs to be set in the Mathewson 1 as part of re-abandonment efforts are detailed in **Table 3.10**. A wellbore diagram displaying the current configuration of the Mathewson 1 as abandoned in 1987 is provided in **Figure 3.40**.

Figure 3.41 provides a diagram of the proposed post-reabandonment configuration of the well.

Table 3.10—Mathewson 1 remedial cement plug details.

Plug	Plug Description	Top (ft)	Bottom (ft)	Length (ft)	Hole Size (in.)	Cement Volume (ft^3)	Notes
[redacted]							

Re-Abandonment Procedure

Class Blowout Preventer:

Class II, 2M blowout preventer (BOP)

Pre-Rig Safety Requirements:

1. Company representative to visit location to ensure equipment access and visually verify all requirements prior to abandonment operations.
2. Verify location of pre-existing surface casing and dry hole marker with ground penetrating radar and/or GPS coordinates from prior abandonment documentation.
3. Inspect wellsite walking surfaces, overhead power line issues, visually ensure location has enough room for rig access, backing in and rig up.
4. Verify anchors are installed and tested.

Abandonment Program Fluids:

Cement to be used:

[redacted]

[redacted].

[redacted]

[redacted]

Abandonment Operations:

[redacted]

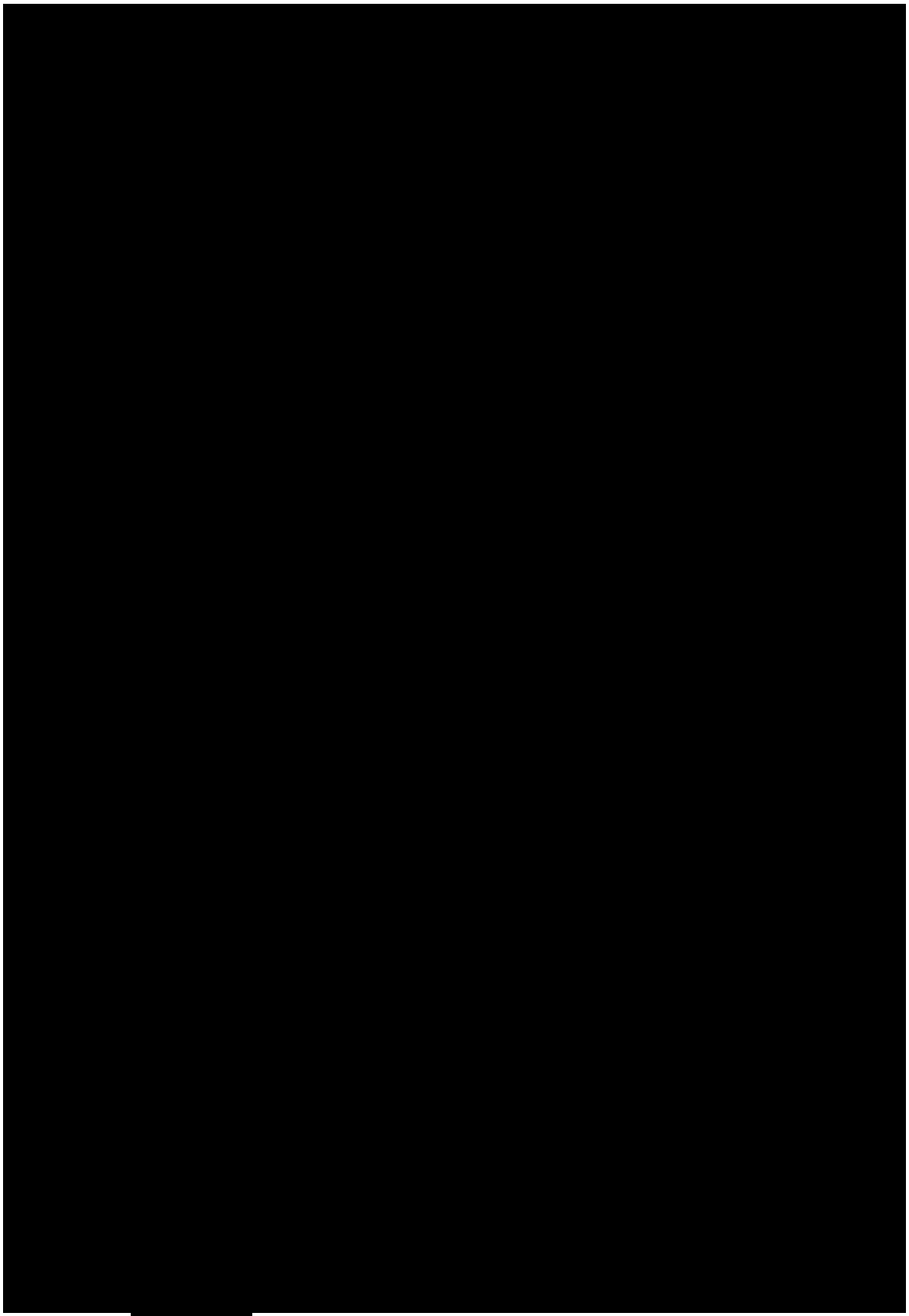

Figure 3.40— [redacted] current configuration wellbore diagram.

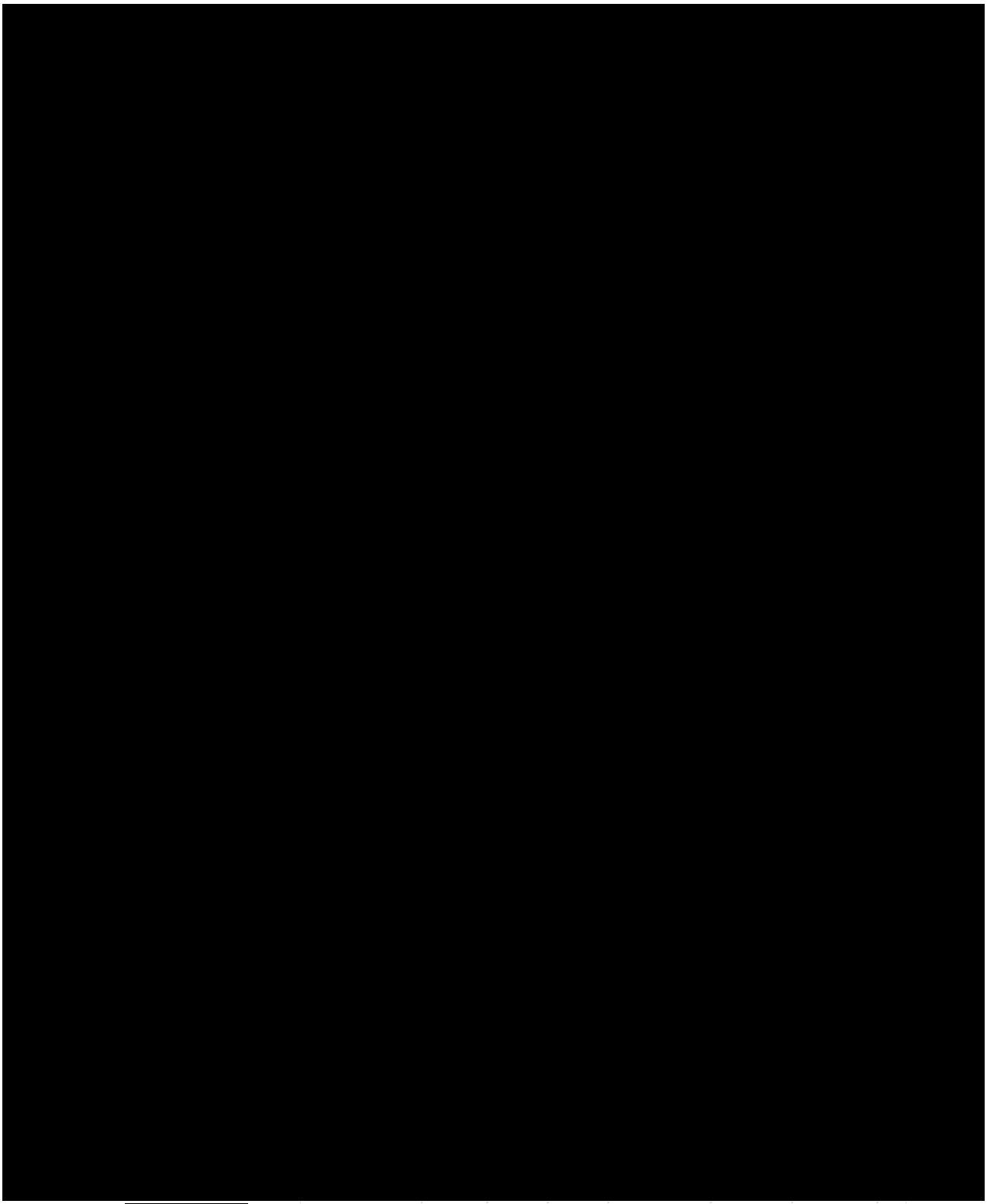

Figure 3.41— [redacted] proposed corrective action re-abandonment.

3.4.2 Plan for Site Access

The State of Nebraska has confirmed ownership of the well and will facilitate access to the wellbore prior to scheduled work. Additionally, High Plains is collaborating with the landowners to ensure road access to the location.

3.4.3 Corrective Action Schedule

While the injectate plume is not predicted to reach the [redacted] until approximately [redacted] years after the start of injection (**Figure 3.36**), the re-abandonment of [redacted] will occur prior to commencing injection into the Conestoga I-1 but following the issuance of a Permit to Construct for the Project.

As the [redacted] is the only penetration of the confining zone within the AoR and the only well requiring corrective action, no phased corrective action is planned.

If the results of testing and monitoring and/or a future AoR re-evaluation (described in the next section) result in the AoR increasing in area, all additional artificial penetrations will be evaluated as above to determine if they penetrate the upper confining zone. If a penetration is identified, it will be thoroughly reviewed to determine whether corrective action is required. Should remediation be necessary, a plan will be developed, and a schedule will be proposed and submitted to the Program Director as part of the AoR re-evaluation. High Plains will guarantee site access is maintained for any future corrective action.

3.5 Re-evaluation Schedule and Criteria

3.5.1 Area of Review Re-evaluation Cycle

As required, High Plains will re-evaluate the above-described AoR every five years during the injection and post-injection phases. The procedure used to reevaluate the AoR will be based on the testing and monitoring data collected between reevaluations and the well conditions at the time of reevaluation.

Future sensitivity analyses will help identify model parameters that drive the largest changes in the plume and AoR size. Changes to the input parameters will be entered into the model, and the impact on the AoR and plume size will be calculated incrementally from each change. Each incremental change will then be compared to the original AoR or further sensitized for uncertainty.

AoR reevaluations will discuss the following:

- Changes to the monitoring and operational data prior to the scheduled reevaluation date.
- How monitoring and operational data (e.g., injection rate and pressure) will be used to update the geologic model and the computational simulations to determine the AoR.

3.5.2 Triggers for AoR Re-evaluations Prior to the Next Scheduled Re-evaluation

The following changes or observations will trigger an AoR re-evaluation prior to the next scheduled reevaluation:

- Significant changes in injection rates or pressures.

- Injection wells added/removed from the Project.
- Determination of the plume growing faster or in a manner inconsistent with earlier model results.

Any observations or measured data deemed to have a material impact on the plume size or AoR will trigger a re-evaluation of the AoR model. Once the injection well is drilled and the new data is acquired and analyzed, the static and dynamic models will be updated, and the AoR will be revised as necessary. Any newly identified wells within the updated AoR will be assessed to determine if corrective action is required. If corrective action is necessary, it will be conducted using methods designed to prevent fluid migration into or between USDWs, including the use of materials compatible with the carbon dioxide stream where appropriate. An amended AoR and corrective action plan will be submitted, or, if no changes to the AoR are warranted, the supporting data and modeling results will be provided.

High Plains will discuss such events with the UIC Program Director to determine if an AoR re-evaluation is required. If an unscheduled re-evaluation is triggered, High Plains will perform the steps described above.

3.6 References

Bartos, T.T., Galloway, D.L., Hallberg, L.L., and others, 2021, Geologic and hydrogeologic characteristics of the White River Formation, Lance Formation, and Fox Hills Sandstone, northern greater Denver Basin, southeastern Laramie County, Wyoming: U.S. Geological Survey Scientific Investigations Report 2021–5020, 219 p., 1 pl., https://doi.org/10.3133/sir20215020.

Bennion, D.B., and Bachu, S., 2007, Permeability and relative permeability measurements at reservoir conditions for CO_2-water systems in ultralow-permeability confining caprocks: Paper presented at the EUROPEC/EAGE Conference and Exhibition, London, U.K., June 2007, https://doi.org/10.2118/106995-MS.

Bennion, D.B., and Bachu, S., 2008, Drainage and imbibition relative permeability relationships for supercritical CO_2/brine and H_2S/brine systems in intergranular sandstone, carbonate, shale, and anhydrite rocks: SPE Reservoir Evaluation & Engineering, v. 11, p. 487-496, https://doi.org/10.2118/99326-PA.

Black, J., Carroll, S., and Haese, R., 2015, Rates of mineral dissolution under CO_2 storage conditions: *Chemical Geology*, v. 399, p. 134-144, https://doi.org/10.1016/j.chemgeo.2014.09.020.

Chang, Y.-B., Coats, B., and Nolen, J., 1998, A compositional model for CO_2 floods including CO_2 solubility in water: *SPE Reservoir Evaluation & Engineering*, v. 1, no. 2, p. 155-160, https://doi.org/10.2118/35164-PA.

Computer Modelling Group Ltd. (CMG), 2024, CMG Builder User Guide: Computer Modelling Group Ltd., Calgary, Alberta, Canada.

Hall, H.N., 1953, Compressibility of reservoir rocks: Technical Note 149, v. 198, https://doi.org/10.2118/953309-G.

Harvey, A.H., 1996, Semiempirical correlation for Henry's constants over large temperature ranges: *AIChE Journal*, v. 42, p. 1491-1494, https://doi.org/10.1002/aic.690420531.

Juanes, R., Spiteri, E., Orr, F.M., and Blunt, M.J., 2006, Impact of relative permeability hysteresis on geological CO_2 storage: *Water Resources Research*, v. 42, no. 12, W12418, https://doi.org/10.1029/2005WR004806.

Kendigelen, O., Egenhoff, S., Matthews, W.A., Holm-Denoma, C.S., Whiteley, K.R., Gent, V.A., Longman, M.W., and Hagadorn, J.W., 2023, The edge of a Permian erg: Eolian facies and provenance of the Lyons Sandstone in northern Colorado: *Rocky Mountain Geology*, v. 58, no. 2, p. 57-82, https://doi.org/10.24872/rmgjournal.58.2.57.

Kestin, J., Khalifa, H.E., and Correia, R.J., 1981, Tables of the dynamic and kinematic viscosity of aqueous NaCl solutions in the temperature range 20–150 °C and the pressure range 0.1–35 MPa: *Journal of Physical and Chemical Reference Data*, v. 10, p. 71-88, https://doi.org/10.1063/1.555641.

Lee, M.-K., and Bethke, C.M., 1994, Groundwater flow, late cementation, and petroleum accumulation in the Permian Lyons Sandstone, Denver Basin: *AAPG Bulletin*, v. 78, no. 2, p. 217–237, https://doi.org/10.1306/BDFF9064-1718-11D7-8645000102C1865D.

Miller, J.A., and Appel, C.L., 1997, Ground Water Atlas of the United States: Segment 3, Kansas, Missouri, Nebraska: U.S. Geological Survey Hydrologic Atlas 730-D, 1 sheet, https://doi.org/10.3133/ha730D.

Oldham, D.W., 1996, Permian salt in the Northern Denver Basin: Controls on occurrence and relationship to oil and gas production from Cretaceous reservoirs, in Longman, M.W., and Sonnenfeld, M.D., eds., *Paleozoic systems of the Rocky Mountain region*: Society for Sedimentary Geology, Rocky Mountain Section, p. 335-354.

Oldham, D.W., 1997, Influence of Permian salt dissolution on Cretaceous oil and gas entrapment, Denver Basin: Graduate Theses, Dissertations, and Problem Reports, West Virginia University, Paper 9535.

Palandri, J.L., and Kharaka, Y.K., 2004, A compilation of rate parameters of water-mineral interaction kinetics for application to geochemical modeling: U.S. Geological Survey Open-File Report 2004-1068, 70 p., https://doi.org/10.3133/ofr20041068.

Peng, D.Y., and Robinson, D.B., 1976, A new two-constant equation of state: *Industrial & Engineering Chemistry Fundamentals*, v. 15, p. 59-64, https://doi.org/10.1021/i160057a011.

Prosper, 2024, *Prosper Performance Update, July 2024*, https://www.prosper.com/blog/prosper-performance-update-july-2024.

Rowe, A.M., and Chou, J.C.S., 1970, Pressure-volume-temperature-concentration relation of aqueous NaCl solutions: Journal of Chemical & Engineering Data, v. 15, p. 61-66, https://doi.org/10.1021/je60044a016.

Sibray, S., Hallum, D.R., Reedy, J., Yuill, J., and Kuntz, T., 2020, Mapping the base of the High Plains Aquifer using borehole geophysical logs and airborne electromagnetic surveys in western Nebraska: University of Nebraska-Lincoln, Conservation and Survey Division, Open File Report 210, 21 p.

Sonnenberg, S.A., 1981, Tectonics, sedimentation, and petroleum potential, northern Denver Basin, Colorado, Wyoming, and Nebraska, Colorado School of Mines, Arthur Lakes Library.

U.S. Department of Commerce, National Institute of Standards and Technology (NIST), 2024, Thermophysical properties of fluid systems, available at https://webbook.nist.gov/chemistry/fluid/.

Zhang, D., and Song, J., 2014, Mechanisms for geological carbon sequestration: Procedia IUTAM, v. 10, p. 319-327, https://doi.org/10.1016/j.piutam.2014.01.027.

APPENDIX 3.1—LIST OF WELLS USED TO CONSTRUCT THE STATIC MODEL

Well Name	API No.	Lat. (NAD83)	Lon. (NAD 83)
[redacted]			

Well Name	API No.	Lat. (NAD83)	Lon. (NAD 83)
[redacted]			

Well Name	API No.	Lat. (NAD83)	Lon. (NAD 83)
[redacted]			

Well Name	API No.	Lat. (NAD83)	Lon. (NAD 83)
[redacted]			

Well Name	API No.	Lat. (NAD83)	Lon. (NAD 83)
[redacted]			

Well Name	API No.	Lat. (NAD83)	Lon. (NAD 83)
[redacted]			

Well Name	API No.	Lat. (NAD83)	Lon. (NAD 83)
[redacted]			

Plan revision number: 1
Plan revision date: 1/31/2025

APPENDIX 3.2—LIST OF OIL AND GAS WELLS WITHIN THE AREA OF REVIEW

API10	Well Name	Operator	Status	PLSS Location (Sec-Twn-Rng)	Surface Latitude (NAD27)	Surface Longitude (NAD27)	Date Spud	Date Completion	Date Abandonment	Field Name	Formation at TD	KB Elev. (ft, msl)	GL Elev. (ft, msl)	TD (ft)	Drill Type
[redacted]															

Plan revision number: 1
Plan revision date: 1/31/2025

API10	Well Name	Operator	Status	PLSS Location (Sec-Twn-Rng)	Surface Latitude (NAD27)	Surface Longitude (NAD27)	Date Spud	Date Completion	Date Abandonment	Field Name	Formation at TD	KB Elev. (ft, msl)	GL Elev. (ft, msl)	TD (ft)	Drill Type
[redacted]															

Plan revision number: 1
Plan revision date: 1/31/2025

API10	Well Name	Operator	Status	PLSS Location (Sec-Twn-Rng)	Surface Latitude (NAD27)	Surface Longitude (NAD27)	Date Spud	Date Completion	Date Abandonment	Field Name	Formation at TD	KB Elev. (ft, msl)	GL Elev. (ft, msl)	TD (ft)	Drill Type
[redacted]															

Plan revision number: 1
Plan revision date: 1/31/2025

API10	Well Name	Operator	Status	PLSS Location (Sec-Twn-Rng)	Surface Latitude (NAD27)	Surface Longitude (NAD27)	Date Spud	Date Completion	Date Abandonment	Field Name	Formation at TD	KB Elev. (ft, msl)	GL Elev. (ft, msl)	TD (ft)	Drill Type
[redacted]															

Plan revision number: 1
Plan revision date: 1/31/2025

API10	Well Name	Operator	Status	PLSS Location (Sec-Twn-Rng)	Surface Latitude (NAD27)	Surface Longitude (NAD27)	Date Spud	Date Completion	Date Abandonment	Field Name	Formation at TD	KB Elev. (ft, msl)	GL Elev. (ft, msl)	TD (ft)	Drill Type
[redacted]															

Plan revision number: 1
Plan revision date: 1/31/2025

API10	Well Name	Operator	Status	PLSS Location (Sec-Twn-Rng)	Surface Latitude (NAD27)	Surface Longitude (NAD27)	Date Spud	Date Completion	Date Abandonment	Field Name	Formation at TD	KB Elev. (ft, msl)	GL Elev. (ft, msl)	TD (ft)	Drill Type
[redacted]															

Plan revision number: 1
Plan revision date: 1/31/2025

	PLSS Location	Surface Latitude	Surface Longitude	Date	Date	Date	Field	Formation	KB Elev.	GL Elev.	TD	Drill
[redacted]												

Well Status Definitions:
ABD-GW – Abandoned Gas Producer
ABD-IW – Abandoned Injection Well
ABD-OW – Abandoned Oil Producer
D&A – Dry & Abandoned
D&A-G – Dry & Abandoned - Gas Shows
D&A-O – Dry & Abandoned - Oil Shows
D&A-OG – Dry & Abandoned - Oil & Gas Shows
OIL – Oil Well
TA-OIL – Temporarily Abandoned - Oil Shows